UNIVERSITY OF CALIFORNIA SAN DIEGO

CAP-Independent Translation of PUMA-α in Apoptotic Response to DNA Damage

A Thesis submitted in partial satisfaction of the
requirements for the degree Master of Science

in

Biology

by

David Sang Tran

Committee in charge:

Professor Jean Y.J. Wang, Chair
Professor Alisa Huffaker, Co-Chair
Professor Katherine Petrie

2021

The Thesis of David Sang Tran is approved, and it is acceptable in quality and form for publication on microfilm and electronically.

University of California San Diego

2021

TABLE OF CONTENTS

LIST OF ABBREVIATIONS

Abbreviations	Definitions
ΔPAPR1	cleaved PARP1
5-FU	5-fluorouracil
5'-RACE	5'-rapid amplification of cDNA ends
aa	amino acid
bGHpA	bovine growth hormone polyadenylation signal
C	clone
cBh	chicken β-actin promoter with hybrid intron
cC	control clone
DMSO	dimethyl sulfoxide
DSB	double stranded break
eFLUT	endogenous fluorescent tagging
FBS	fetal bovine serum
G418	geneticin
HDR	homology directed repair
HRP	horseradish peroxidase
IAP	inhibitor of apoptosis
KO	knockout
LB	luria broth
MLS	mitochondrial localization signal
MOMP	mitochondrial outer membrane permeabilization
NBI	normalized band intensity
NHEJ	non-homologous end joining
NLS	nuclear localization signal
ORF	open reading frame
P	parental
PARP	poly ADP-ribose polymerase
PBS	phosphate buffered saline
PUMA	p53 upregulated mediator of apoptosis
Puro	puromycin resistance gene
PVDF	polyvinylidene fluoride
RNAi	RNA interference
sgRNA	single guide RNA
shRNA	short hairpin RNA
siRNA	small interfering RNA
TBST	tris-buffered saline
TM	transmembrane domain
uORF	upstream open reading frame
VpN	venus_p2a_neo
WCL	whole cell lysate
YFP	yellow fluorescent protein

LIST OF FIGURES

LIST OF TABLES

ACKNOWLEDGEMENTS

I would like to thank my mentor, Professor Jean Wang, for guiding and supporting me throughout my MS study. Professor Wang has taught me many invaluable lessons in and outside of the laboratory environment that has help me grow not only as a scientist, but also as a person. My completion of the BS/MS program would not have been possible without her patience, guidance, and generosity. I will always be grateful for the learning opportunity she has given me.

I would also like to thank my committee members: Professor Huffaker and Professor Petrie for their support through this process as well as the entire Kolodner Lab researchers for their assistance and encouragement.

Lastly, I would like to thank my parents, family, and friends for always supporting me at every step and for being there when I needed them most.

ABSTRACT OF THE THESIS

CAP-Independent Translation of PUMA-α in Apoptotic Response to DNA Damage

by

David Sang Tran

Master of Science in Biology

University of California San Diego, 2021

Professor Jean Y.J. Wang, Chair
Professor Alisa Huffaker, Co-Chair

DNA damage induces the expression of **p**53-**u**pregulated-**m**ediator-of-**a**poptosis (PUMA-α) to activate the intrinsic apoptosis pathway. Our lab has shown that cisplatin induces *PUMA-α* mRNA without increasing PUMA-α protein or apoptosis in renal epithelial cells of mice with germline mutations to block nuclear import of Abl-tyrosine kinase. This finding suggests that *PUMA-α* translation is also regulated in DNA damage response. Inspection of *PUMA-α* sequence reveals an upstream open reading frame (uORF), which if translated, may interfere with translation from the downstream AUG of the *PUMA-α* ORF. To determine if this uORF is

translated, I inserted a Venus_p2a_Neo ORF using CRISPR/Cas9 technology into *PUMA-α Exon-1a* to increase the uORF coding capacity from 41 aa to a 577 aa. Following selection for neomycin-resistance and single-cell cloning, I detected Venus expression by fluorescence microscopy and Neo expression by immunoblotting in several edited cell clones, supporting translation of the uORF and suggesting *PUMA-α* is translated from an internal AUG, which can occur through Leaky Scanning (CAP-dependent) or Re-initiation (CAP-independent). To distinguish between these two mechanisms, I treated cells with 4EGI-1, an inhibitor of CAP-dependent translation and a DNA damaging agent separately or in combination, and found that 4EGI-1 reduced p53 and p21CIP1 but not PUMA-α protein levels. Together, the findings that the uORF is translated and that 4EGI-1 does not reduce PUMA-α protein strongly suggest that *PUMA-α* translation is driven by CAP-independent re-initiation and support future investigation to solve the nuclear Abl-dependent translation re-initiation mechanism for PUMA-α expression.

CHAPTER 1 INTRODUCTION

1.1 Defect in DNA Damage Induced Apoptosis as a Hallmark of Cancer Cells

The hallmarks of cancer, i.e., the pathogenic mechanisms that drive tumorigenesis, are (a) sustained proliferative signaling, (b) evading growth suppressors, (c) resisting cell death, (d) enabling replicative immortality, (e) inducing angiogenesis, and (f) activating invasion and metastasis, which are malignant phenotypes shared by all cancers (Hanahan et al., 2000; Hanahan et al., 2011; Weinberg, 1989). Underlying these pathogenic mechanisms are the genetic and epigenetic alterations in the expression and the functions of oncogenes and tumor suppressor genes that regulate cell proliferation and cell death. Studies of the genetic basis for cancer predisposition in humans have discovered many tumor suppressor genes in which loss-of-function germline mutations cause early onset of cancers in patients who have inherited a tumor suppressor mutation (Dryja et al., 1986; Friend et al., 1986; Fung et al., 1987; Knudson, 1971; Lee et al., 1987). Among the human tumor suppressor genes is the *TP53* gene that is mutated in patients of the Li-Fraumeni syndrome (Malkin, 1991; Frebourg, 1995), and in at least half of sporadic human cancers not related to the Li-Fraumeni syndrome (Hollstein et al., 1991). Even in cancer cells with wild-type *TP53*, the p53-functions are inactivated by alternative mechanisms, such as the over-expression of MDM2, which is an E3-ubiquitin ligase that targets p53 for proteasome degradation (Haupt et al., 1997; Ute et al., 2003). The *TP53* gene encodes a transcription factor p53 that is activated by DNA damage, among other stress signals, to orchestrate gene expression responses that either inhibit proliferation or promote cell death (Oren, 1999; Fischer, 2017). Therefore, loss of p53 function in cancers contributes to the resistance of cancer cells to stress-induced cell cycle arrest and apoptosis (Haupt et al., 1997).

Despite the loss of p53, however, DNA damaging agents such as radiation and chemotherapy drugs have been used to treat cancers for almost a century, showing that DNA damage can activate p53-independent growth arrest or cell death in cancer cells. It turns out that *TP53* is a member of a family of transcription factors that include p53, p63, and p73 (Jost et al., 1997; Levrero et al., 2000; Yang et al., 1998). This p53/p63/p73-family of transcription factors bind to similar DNA sequences and therefore regulate a similar set of genes (Kaghad et al., 1997; Levrero et al., 2000; Yang et al., 1998). It has been demonstrated that DNA damage not only activates p53, but also activates p63 and p73 (Gong et al., 1999; Jost et al., 1997; Levrero et al., 2000; Yang et al., 1998). Among the genes that are commonly regulated by the p53/p63/p63 family of transcription factors is *CDKN1A*, which encodes $p21^{Waf1/Cip1}$ protein that binds to and inhibits the activities of CDK2-cyclin complexes to cause cell cycle arrest (Harper et al., 1993); Harper et al., 1995; Zhu et al., 2005). Another common target gene for p53/p63/p73 is *BBC3*, which encodes PUMA-α (p53-upregulated mediator of apoptosis) to activate intrinsic apoptosis (Nakano et al., 2001; Yu et al., 2001). Since p63 and p73 are seldom mutated in cancers, possibly because these two members of the family have functions that contribute to the maintenance of stem-ness in cancer cells, their functions could account for the p53-independent cancer cell death response to radiation and chemotherapy.

While radiation and chemotherapy have been successful in curing some cancer types, particularly, childhood cancer, these DNA damaging agents fail to treat the majority of adult solid tumors due to the emergence of cancer cells that are resistant to DNA damage-induced cell death. Since resistance cancer cells do not appear to inactivate the *TP63*, the *TP73*, and the *BBC3* genes, other mechanisms such as enhanced DNA repair, increased expression of anti-apoptotic proteins, and reduced expression of pro-apoptotic proteins such as PUMA-α may contribute to

cancer resistance to genotoxic therapies (Dotsch et al., 2010). Understanding the mechanisms by which cancer cells evade DNA damage-induced cell death despite the wild-type status of p63 and p73 is of value for such knowledge can contribute to the development of rational strategies to enhance the efficacy of radiation and chemotherapy.

1.2 The *BBC3* Gene, Transcripts, Proteins, and Their Roles in DNA Damage Induced Apoptosis.

The PUMA-α transcript encoded by the *BBC3* gene was first discovered in 2001 by two independent laboratories interested in identifying p53-regulated mRNAs that are required for the stimulation of apoptosis (Nakano et al., 2000; Yu et al., 2001). They named this transcript *PUMA* (p53 upregulated mediator of apoptosis) due to its p53-dependent transcription and its potent proapoptotic activity. The Yu et al group found that the PUMA protein is exclusively localized to the mitochondria and binds to Bcl-2 and Bcl-X_L through its BH3 domain (Yu et al., 2001). They also showed that ectopic expression of PUMA induced apoptosis that occurred at a faster rate than that induced by the ectopic expression of p53 (Yu et al., 2001). The Nakano et al group identified two PUMA-isoforms, namely PUMA-α and PUMA-β, with both proteins containing the pro-apoptotic BH3 domain, capable of binding to Bcl-2, localizing to the mitochondria, inducing cytochrome c release, and activating the rapid induction of intrinsic apoptosis. In summary, the two groups independently identified *PUMA* as a p53-induced transcript, that is induced by DNA damage in p53-proficient, but not in p53-deficient cells, and that the ectopic expression of PUMA is sufficient to kill p53-deficient cancer cells.

We now know that PUMA is encoded by the *BBC3* gene that is mapped to the q arm of human chromosome 19. The *PUMA* transcript discovered by Yu et al. is now known as PUMA-

α, which is one of four protein-coding mRNAs transcribed from the *BBC3* gene: namely, PUMA-β, PUMA-γ and PUMA-δ (Figure 1.1). Only the PUMA-α and PUMA-β proteins contain the pro-apoptotic BH3 domain, whereas the biological functions of PUMA-γ and PUMA-δ have not been investigated. The PUMA-α transcript consists of four exons (1a, 2, 3, 4), transcribed from an internal promoter that is unique to this isoform, and with the translation initiation codon for the PUMA-α protein located in exon 2 (Figure 1.1). Two p53-binding sites, located at 230 and 144 base pairs of the *PUMA-α* transcription start site, have been shown to mediate p53-independent upregulation of *PUMA-α* mRNA (Yu et al., 2001).

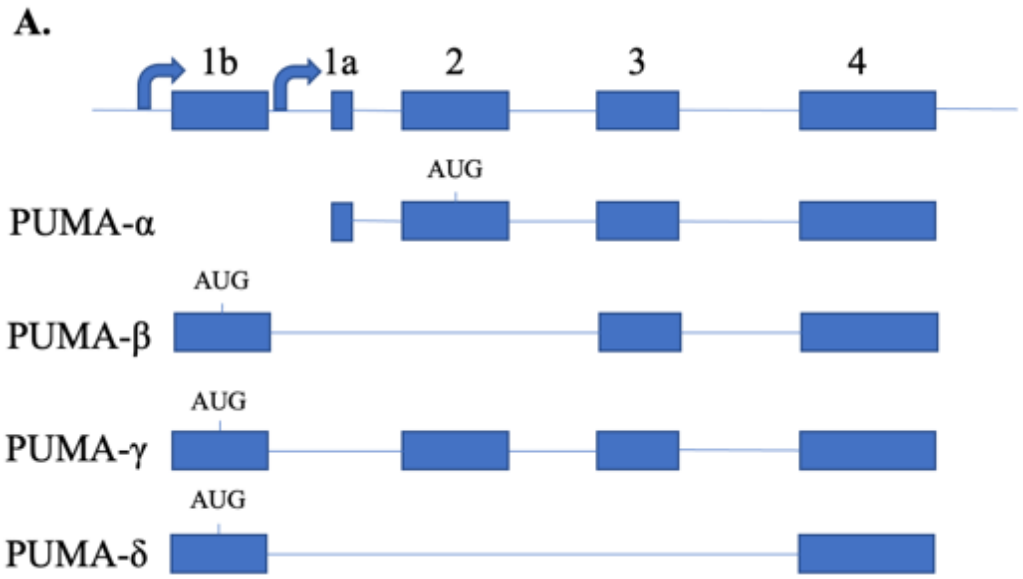

B.

PUMA-α

MARARQEGSSPEPVEGLARDGPRPFPLGRLVPSAVSCGL
CEPGLAAAPAAPTLLPAAYLCAPTAPPAVTAALGGSRWP
GGPRSRPRGPRPDGPQPSLSLAEQHLESPVPSAPGALAGG
PTQAAPGVRGEEEQWAREIGAQ**LRRMADDLN**AQYERR
RQEEQQRHRPSPWRVLYNLIMGLLPLPRGHRAPEMEPN

PUMA-β

MKFGMGSAQACPCQVPRAASTTWVPCQICGPQPSLSLA
EQHLESPVPSAPGALAGGPTQAAPGVRGEEEQWAREIGA
Q**LRRMADDLN**AQYERRRQEEQQRHRPSPWRVLYNLIM
GLLPLPRGHRAPEMEPN

PUMA-γ

MKFGMGSAQACPCQVPRAASTTWVPCQICGPRERHGPR
TPGGQLPGARRGPGPRRPAPLPARPPGALGSVLRPLRAR
PGCRPRRPHPAARCLPLRPHRPTRRHRRPGGFPLAWGSP
QPAPRPAPGRSSALALAGGAAPGVARAQRPGGSGGRSH
PGGPGSPRGGGTVGPGDRGPAAADGGRPQRTVRAAETR
GAAAAPPLTLEGPVQSHHGTPALTQGPQSPRDGAQLGA
CTRPVDVRDSGGRPLPPPDTLASAGDFLCTM

PUMA-δ

MKFGMGSAQACPCQVPRAASTTWVPCQICETRGAAAAP
PLTLEGPVQSHHGTPALTQGPQSPRDGAQLGACTRPVDV
RDSGGRPLPPPDTLASAGDFLCTM

Figure 1.1 Transcripts and Proteins Encoded by the Human *BBC3* Gene. (A) The exon-intron organization of the four transcripts encoded by the human *BBC* gene. The blue boxes denote the exons, and the two arrows denote the alternative promoters. The alternative promoters and splicing generate four different transcripts, PUMA-α, PUMA-β, PUMA-γ, and PUMA-δ consisting of 1846, 1538, 1827, and 1347 base pairs, respectively. The translation initiation codon (AUG) is marked in each transcript. (B) Amino acid sequences of PUMA-α, PUMA-β, PUMA-γ, and PUMA-δ proteins containing 193, 131, 261, and 101 amino acids, respectively. The pro-apoptotic BH3 domain amino acids, found in PUMA-α and PUMA-β proteins, are bolded and underlined.

PUMA-α protein contains 90 α-specific amino acids (aa) at its N-terminus, a BH3 domain and a transmembrane domain (TM) at its C-terminus required from insertion into the mitochondrial outer membrane (Hikisz et al., 2012). The BH3 and the TM domains are both required for PUMA-α to activate intrinsic mitochondria-dependent apoptotic pathways (Evan & Vousden, 2001). The BH3 domain of PUMA-α binds to the hydrophobic pockets of the anti-apoptotic proteins such as Bcl-x, Bcl-2, A1, and Bcl-B to prevent these anti-apoptotic proteins from binding BAX and BAK, the effectors of apoptosis (Fischer, 2017). The activated BAX and BAK form oligomeric channels in the mitochondrial outer membrane to cause mitochondrial outer membrane permeabilization (MOMP). MOMP allows for the release of cytochrome c and Smac/Diablo and other apoptosis inducers form the mitochondria (Norbury & Zhivotosky, 2004). In the cytoplasm, cytochrome c binds to and activates the adapter protein Apaf-1 to oligomerize with pro-caspase-9 to form the apoptosome (Norbury & Zhivotosky, 2004). This activates Caspase-9 which in turn activates caspases-3 and caspases-7. In parallel, the release Smac/Diablo blocks the inhibitor of apoptosis proteins (IAPs) to prevent IAPs from inhibiting the activated caspases (Norbury & Zhivotosky, 2004). The activated caspases-3 and -7 then cleave numerous cellular components to cause chromatin condensation, DNA fragmentation, cell shrinkage, externalization of phosphotidyl-serine to stimulate engulfment of fragmented apoptotic bodies (Norbury & Zhivotosky, 2004).

The pro-apoptotic function of PUMA-α has been demonstrated in vivo by the constructions and analyses of PUMA-knockout (KO) mice. Thymocytes from PUMA KO mice are as resistant as those from *TP53*-KO mice to etoposide or γ radiation induced apoptosis (Villunger et al., 2003). PUMA-KO in C57/B6 mice also significantly increased mice survival following 15 Gy whole-body-irradiation to cause gastrointestinal damage (Leibowitz et al.,

2011). These results show that in some tissues and cell types, including thymocytes, neuroblasts, renal epithelial cells, and intestinal cells, loss of PUMA is as effective as loss of p53 in reducing apoptosis to DNA damage.

1.3 Upstream Open Reading Frames in the Regulation of Translation

In eukaryotes, mRNA translation typically occurs from the 5'most initiation codon (AUG or GUG). This is in contrast with prokaryotic translation, where an mRNA can carry multiple open reading frames (ORFs) with ribosomes capable of successive re-initiations of translation from internal initiation codons. However, recent studies have found that many mammalian mRNAs also carry multiple ORFs, and those occurring upstream of the protein coding ORFs, i.e., uORFs, can regulate the translation of downstream protein coding sequences (Young et al., 2016). In canonical CAP-dependent translation initiation, the eIF4F complex is recruited to the m7 G CAP structure at the 5' end of mRNAs to position the 43S ribosome complex for translation initiation (Sriram et al., 2018). This eIF4F complex consists of four components: (1) eIF4E which binds to the m7G-CAP, (2) eIF4A which helps unwind the 5' region of the mRNA, (3) eIF4B which stimulates the activity of eIF4A, and (4) eIF4G which is the main scaffolding subunit that interacts with eIF4E and recruits the 43S pre-initiation complex by binding eIF3 and circularizing the mRNA by binding poly(A)-binding proteins (Sriram et al., 2018). The 43S pre-initiation complex, consisting of the ternary complex and the 40S ribosome and positioned at the 5'CAP then scans along the mRNA in a 5' to 3' direction to initiate translation at the most proximal AUG or GUG codon (Sriram et al., 2018). After dissociation from the termination codon, the 80S eukaryotic ribosome cannot re-initiate translation from an internal AUG or GUG codon due to the absence of the CAP-structure. Recent studies have discovered that translation from an internal AUG or GUG can occur in eukaryotic cells through Leaky Scanning or Re-

initiation (Sriram et al., 2018). In Leaky Scanning, ribosomes are loaded onto the mRNA via the 5'CAP but then skip the most proximal AUG to start translation at an internal AUG (Sriram et al., 2018). This may occur if the upstream AUG is part of a small uORF which does not code for a protein or peptide of biological function. In Re-initiation, ribosomes are loaded onto the internal AUG through mechanisms that do not require the 5'-CAP (Sriram et al., 2018). Potential mechanisms that re-initiate translation from internal AUG or GUG include the recruitment of canonical translation initiation factors eIF3h and non-canonical initiation factors eIF2D, DENR, and MCTS1 (Sriram et al., 2018).

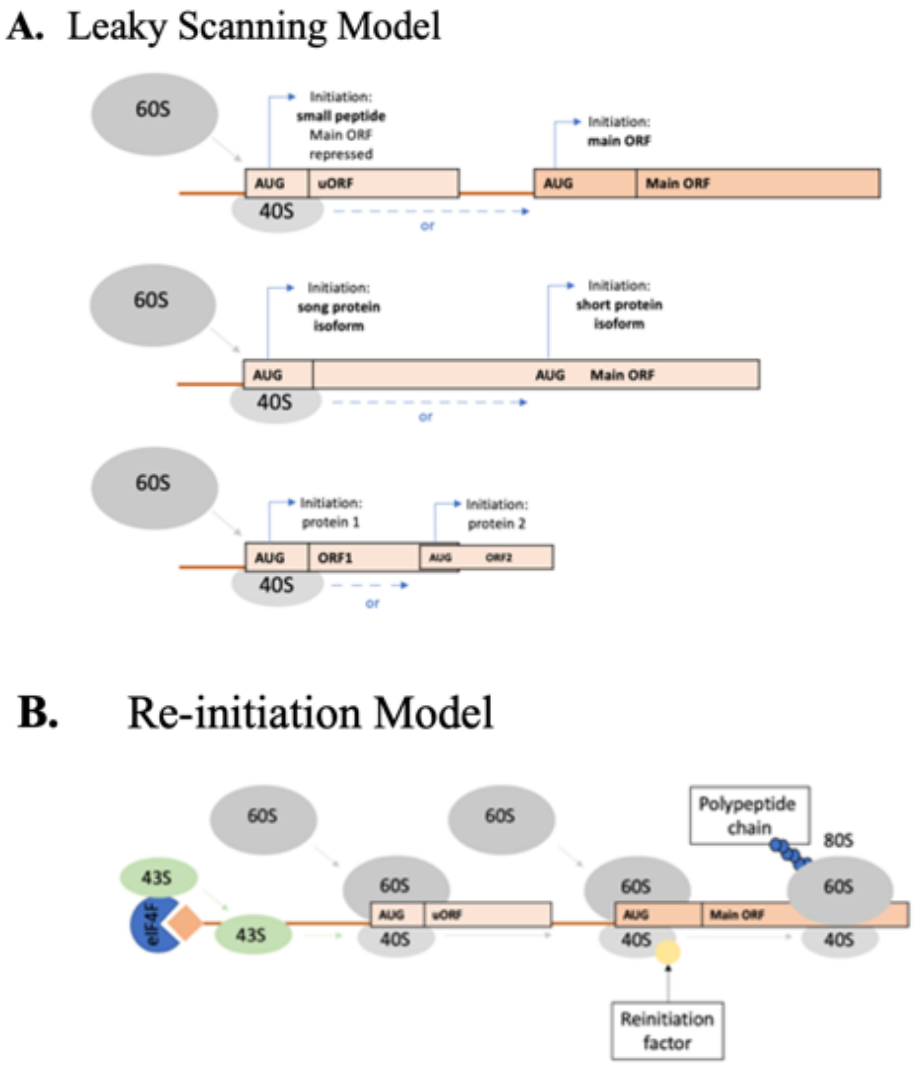

Figure 1.2 Mechanisms for Translation from the Internal AUG of PUMA-α. (A) Leaky Scanning Model for Internal AUG Translation. With the Leaky Scanning Model, ribosomes are loaded onto the mRNA via the 5'-CAP but skip the most proximal AUG and begins translation at an internal AUG. (B) Re-initiation Model for Internal AUG Translation. In the Re-initiation Model, ribosomes are loaded onto the internal AUG through mechanisms that do not involve recognition of the 5'-CAP, such as a reinitiation factor.

1.4 Experimental Questions and Approaches

Previous studies have found that *PUMA-α* mRNA induction in Abl-nuclear import-defective mouse kidney epithelial cells exposed to cisplatin did not lead to PUMA-α protein accumulation (Sridevi et al., 2013). As a result, cisplatin-induced increase in *PUMA-α* mRNA was not sufficient to activate apoptosis in Abl-nuclear import defective kidney epithelial cells (Sridevi et al., 2013). Those *in vivo* results suggested that PUMA-α translation may be additionally regulated, in a nuclear Abl-dependent manner, to determine the apoptotic response to DNA damage. Inspection of the *PUMA-α* mRNA sequences in several genomic databases has shown that the open-reading frame (ORF) of PUMA-α begins with a start codon in Exon 2 and ends with a stop codon in Exon 4. The 1.8 kb mRNA contains 286 nucleotides of un-translated region (UTR) in Exon 1a on the 5'-end and 978 nucleotides of UTR in Exon 4 on the 3'-end. Interestingly, the 5'-UTR of the *PUMA-α* mRNA contains a small ORF of 32 amino acids (aa) with a start codon and a stop codon in Exon 1a of the *PUMA-α* mRNA. This upstream ORF (uORF) is noted in the uORF database, which also finds an uORF in the Exon 1b of the *PUMA-β, γ, δ* mRNAs. The presence of this uORF in the *PUMA-α* mRNA raises the interesting question whether this 32-aa uORF is translated. If the uORF were to be translated, then the translation of PUMA-α ORF would have to initiate from an internal AUG Leaky Scanning or Re-initiation mechanism (Figure 1.2).

To determine if the uORF of PUMA-α is translated, I inserted a Venus_p2a_Neo (VpN) cassette using CRISPR/Cas9 technology into Exon 1a of *BBC3*, positioning the VpN ORF at the C-terminus of the uORF and upstream of the uORF termination codon (Ran et al., 2013; Steward-Ornstein & Lahav, 2016). If the AUG of this uORF is recognized by the ribosome, then the Venus_p2a_Neo (VpN)-edited *BBC3* gene would be expected to encode an expanded uORF

for expression of the Venus fluorescence protein and the Neomycin resistance factor, thus allowing for selection of edited clones by resistance to neomycin and detection of Venus by fluorescence microscopy (Stewart-Ornstein & Lahav, 2016). I isolated and analyzed the expression of Venus and Neo from several single cell clones after editing. I also sequenced the genomic fragments amplified from these single cell clones to verify that the cassette is indeed inserted into Exon 1a of *BBC3*.

As discussed above, translation from an internal AUG in eukaryotic cells can be mediated by CAP-dependent Leaky Scanning or CAP-independent Re-initiation (Figure 1.2). To distinguish between these two different mechanisms for translation of PUMA-α ORF, I used a compound called 4EGI-1, which blocks the interaction between eIF4E and eIF4G to inhibit CAP-dependent translation. If PUMA-α ORF is translated by Leaky Scanning, then 4EGI-1 would be expected to inhibit the expression of PUMA-α protein. However, if PUMA-α ORF is translated by re-initiation, then 4EGI-1 would not be able to inhibit the expression of PUMA-α protein.

1.5 References

Barbosa, C., Peixeiro, I., Romao, L. (2013). Gene Expression Regulation by Upstream Open Reading Frames and Human Disease. *PLoS Genet, 9(8),* e1003529. Doi: 10.1371/journal.pgen.1003529

Dotsch, V., Bernassola, F., Coutandin, D., Candi, E., Melino, D. (2010). P63 and p73, the Ancestors of p53. *Cold Spring Harbor Perspectives in Biology. 2(9),* a004887. doi: 10.1101/cshperspect.a004887

Dryja, TP., Rapaport, JM., Joyce, JM., Petersen, RA. (1986). Molecular detection of deletions involving band p14 of chromosome 13 in retinoblastomas. *Proceedings of the National Academy of Sciences of the United States of America, 83,* 7391-7394. doi: 10.1073/pnas.83.19.7391

Evan, GI., Vousden, KH. (2001). Proliferation, cell cycle and apoptosis in cancer. *Nature, 411(6835),* 342-348. doi: 10.1038/35077213

Fernandez, V., Garcia-Murria, M., Bano-Polo, M., Martin, J., Monticelli, L., Orzaez, M., Mingarro, I. (2016). The C-terminal Domains of Apoptotic BH3-only Proteins Mediate Their Insertion into Distinct Biological Membranes. *The Journal of Biological Chemistry, 291(48),* 25207-25216. doi: 10.1074/jbc.M116.733634

Frebourg, T., Barbier, N., Yan, YX., Garber, JE., Dreyfus, M., Fraumeni, J., Li, F., Friend, S. (1995). Germ-line p53 mutations in 15 families with Li-Fraumeni syndrome. Am J Hum Genet, *56(3)*, 608-615. PMID: 7887414

Friend, SH., Bernards, R., Rogelj, S., Weinberg, RA., Rapaport, JM., Alber, DM., Dryja, T. (1986). A human DNA segment with properties of the gene that predisposes to retinoblastoma and osteosarcoma. *Nature, 323,* 643-646. Doi: 10.1038/323643a0

Fung, YKT., Murphree, AL., T'Ang, A., Qian, J., Hinrichs, SH., Benedict, WF. (1987). Molecular biology of the human retinoblastoma gene. *Science, 236,* 1657-1661. doi: 10.1007/978-1-4613-1599-5_13

Fischer, M. (2017). Census and evaluation of p53 target genes. *Oncogene, 36,* 3943-3956. doi: 10.1038/onc.201.502

Gomex, N., Espinosa, J. (2010). Gene-specific repression of the p53 target gene PUMA via intragenic CTCF-Cohesion binding. *Genes and Development, 24,* 1022-1034. doi: 10.1101/gad.1881010

Gong JG., Constanzo, A., Yang., HQ, Melino., G., Kaelin., WG., Levrero., M., Wang, JY. (1999). The tyrosine kinase c-Abl regulates p73 in apoptotic response to cisplatin-induced DNA damage. *Nature, 399(6738),* 806-809. doi: 10.1038/21690

Hanahan, D., Weinberg, R. (2000). The Hallmarks of Cancer. *Cell, 100*, 57-70. doi: 10.1016/s0092-8674(00)81683-9

Harper, JW., Adami, G., Wei, N., Keyomarsi, K., Elledge, SJ. (1993). The p21 Cdk-interacting Protein Cip1 Is a Potent Inhibitor of G1 Cyclin-Dependent Kinases. *Cell, 75,* 805-816. doi: 10.1016/0092-8672(93)90499-g

Harper, JW., Elledge, SJ., Keyomarsi, K., Dynlacht, B., Tsai, LH., Zhang, P., Dobrowolski, S., Bai, C., Connell-Crowley, L., Swindell, E. (1995). Inhibition of cyclin-dependent kinases by p21. *Molecular Biology of the Cell, 6(4),* 387-400. doi: 10.1091/mbc.6.4.387

Haupt, Y., Maya, R., Kazaz, A., Orgen, M. (1997). Mdm2 promotes the rapid degradation of p53. *Nature, 387,* 296-299. doi: 10.1038/387296a0

Hanahan, D., Weinberg, R. (2011). The Hallmarks of Cancer: The Next Generation. *Cell*, *144*, 646-673. doi: 10.1016/j.cell.2011.02.013

Hikisz, P., Kilianska, Z. (2012). PUMA, A Critical Mediator of Cell Death – One Decade on from its Discovery. *Cellular & Molecular Biology Letters. 17,* 46-669. Doi: 10.2478/s11658-012-0032-5

Hollstein, M., Sidransky, D., Volgelstein, B., Harris, C. (1991). p53 Mutations in Human Cancers. *Science, 252(5015),* 49-53. doi: 10.1126/science.1905840

Irwin, MS., Kaelin, WG. (2001). P53 family update: p73 and p63 develop their own identities. *Cell Growth Differentiation, 12(7),* 337-349. PMID: 11457731.

Jost, CA., Marin, MC., Kaelin, WG. (1997). P73 is a simian [correction of human] p53-related protein that can induce apoptosis. *Nature, 389(6647),* 191-194. doi: 10.1038/38298.

Kaghad, M., Bonneet, H., Yang, A., Creacier, L., Biscan, J., Valent, A., Minty, A., Chalon, P., Lelias, J., Durmont, X., Perrara, P., McKeon, F., Caput, D. (1997). Monoallelically expressed gene related to p53 at 1p36, a region frequently deleted in neuroblastoma and other human cancers. *Cell, 90,* 809-819. oi: 10.1016/s0092-8674(00)80540-1

Knudson, AG. (1971). Mutation and Cancer: Statistical Study of Retinoblastoma. *Proceedings of the National Academy of Science of the United States of America, 68(4),* 820-823. doi: 10.1073/pnas.68.4.820

Lee, W-H., Bookstein, R., Hong, F., Young, L-J., Shew, J-Y., Lee, EYHP. (1987). Human retinoblastoma susceptibility gene: cloning, identification, and sequence. *Science, 235,* 1394-1399. doi: 10.1126/science. 3823889.

Leibowitz, B., Qiu, W., Liu, H., Cheng, T., Zhang, L., Yu, J. (2011). Uncoupling p53 Functions in Radiation-Induced Intestinal Damage via PUMA and p21. *Molecular Cancer Research, 9(5),* 616-625. doi: 10.1158/1541-7786.MCR-11-0052

Levrero, M., De Laurenzi, V., Costanzo, A., Gong, J., Wang, JY., Melino, G. (2000). The p53/p63/p73 family of transcription factors: overlapping and distinct functions. *Journal of Cell Science, 113,* 1661-1670. PMID: 10769197.

Malkin, D. (2011). Li-Fraumeni Syndrome. *Genes & Cancer, 2(4),* 475-484. Doi: 10.1177/1947601911413466

Nakano, K., Vousden, K. (2001). *PUMA*, a Novel Proapoptotic Gene, Is Induced by p53. *Molecular Cell, 7,* 683-694. doi: 10.1016/s1097-2765(01)00214-3

Norbury, C., Zhivotovsky, B. (2004). DNA damage-induced apoptosis. *Oncogene, 23,* 2797-2808. doi: 10.1038/sj.onc.1207532

Oren, M. (1999). Regulation of the p53 Tumor Suppressor Protein. *Journal of Biological Chemistry, 274,* 36031-36034. doi: 10.1074/jbc.274.51.36031.

Ran, F. A., Hsu, P. D., Wright, J., Agarwala, V., Scott, D. A., & Zhang, F. (2013). Genome engineering using the CRISPR-Cas9 system. *Nature protocols*, *8*(11), 2281–2308. https://doi.org/10.1038/nprot.2013.143

Sridevi, P., Nhiayi, M., Wang, J. (2013). Genetic disruption of Abl nuclear import reduces renal apoptosis in a mouse model of cisplatin-induced nephrotoxicity. *Cell Death Differentiation, 20(7),* 953-962. doi: 10.1038/cdd.2013.42

Sriram, A., Bohlen, J., Teleman, A. (2018). Translation acrobatics: how cancer cells exploit alternate modes of translation initiation. *EMBO reports, 10,* e45947. doi: 10.15252/embr.201845947

Stewart-Ornstein, J., Lahav, G. (2016). Dynamics of CDKN1A in Single Cells Defined by an Endogenous Fluorescent Tagging Toolkit. *Cell Reports, 14,* 1800-1811. doi: 10.1016/j.celrep.2016.01.045

Ute, M., Petrenko, O. (2003). The MDM2-p53 Interaction. *Molecular Cancer Research, 1,* 1001-1008. PMID: 14707283.

Villunger, A., Michalak, E., Coultas, L., Mullauer, F., Bock, G., Ausserlechner, M., Adams, J., Strasser, A. (2003). p53- and Drug-Induced Apoptotic Responses mediated by BH3-Only Proteins Puma and Noxa. *Science, 302,* 1036-1038. doi: 10.1126/science.1090072.

Weinberg, R. (1989). Oncogenes, Antioncogenes, and the Molecular Bases of Multistep Carcinogenesis. *Cancer Research, 49,* 3713-3721. https://pubmed.ncbi.nlm.nih.gov/2660980/

Yang, A., Kaghad, M., Wang, Y., Gillett, E., Fleming, MD., Dotsch, V., Andrews, NC., Caput, D., McKeon, F. (1998). P63, a p53 homolog at 3q27-29, encodes multiple products with transactivating, death-inducing, and dominant-negative activities. doi: 10.1016/s1097-2765(00)80275-0

Young, S., Wek, R. (2016). Upstream Open Reading Frames Differentially Regulate Gene-specific Translation in the Integrated Stress Response. *The Journal of Biological Chemistry, 291(33),* 16927-16935. doi: 10.1074/jbc.R116.733899

Yu, J., Zhang, L., Hwang, P., Rago, C., Kinzler, K., Vogelstein, B. (1999). Identification and classification of p53-regulated genes. *Proceedings of the National Academy of Sciences of the United States of America, 96(25),* 14517-14522. doi: 10.1073/pnas.96.25.14517

Yu, J., Zhang, L., Hwang, P., Kinzler, K., Vogelstein, B. (2001). PUMA Induces the Rapid Apoptosis of Colorectal Cancer Cells. *Molecular Cell, 7,* 673-682. doi: 10.1016/s1097-2765(01)00213-1

Yu, J., Zhang, L. (2003). No PUMA, no death: Implications for p53-dependent apoptosis. *Cancer Cell, 4(4),* 248-249. doi: 10.1016/S1535-6108(03)00249-6

Yu, J., L, Zhang. (2008). PUMA, a potent killer with or without p53. *Oncogene, 27,* 71-83. doi: 10.1038/onc.2009.45

Zhu, H., Nie, L., Maki, C. (2005). Cdk2-dependent Inhibition of p21 Stability via a C-terminal Cyclin-binding Motif. *Journal of Biological Chemistry, 280(32),* 29282-29288. doi: 10.1074/jbc.M407352200

CHAPTER 2 MATERIALS AND METHODS

2.1 Selection of sgRNAs

The Broad Institute sgRNA Designer (https://portals.broadinstitute.org/gpp/public /analysis-tools/sgrna-design) was used to generate a list of potential single-guide RNAs (sgRNAs) that targeted the *BBC3* gene. sgRNAs that targeted Exon-4 (sgRNA 3/4 & sgRNA 11/12) and Exon-1a (sgRNA 13/14) were selected based on their target site relative to the termination codon in their respective exons, on-target efficacy scores, and off-target rankings. sgRNA 3/4 and sgRNA 11/12 were also selected in pair based on their PAM-out orientation to facilitate double-cutting.

2.2 Preparation of sgRNA-Cas9 Constructs

The procedure used to create sgRNA expression constructs is identical to that described in the Zhang et al paper (Ran et al., 2013). The top and bottom sgRNA oligos for each sgRNA design were annealed and phosphorylated at the 5' ends using T4 PNK. This reaction was subjected to 37˚C for 30 minutes, 95˚C for 5 minutes, and a ramp down to 25˚C at the rate of 5˚C/minute. All temperature and time-based reactions were performed using the GeneAmp PCR System 9700. The phosphorylated and annealed oligos were diluted 1:200. The pSpCas9(BB)-2A-Puro vector was digested using the restriction enzyme Bbsl (Bpil) and incubated with Tango buffer, DTT, and ATP at 37˚C for 1 hour. Next the diluted annealed sgRNA oligos were ligated into the digested vectors using T4 DNA ligase at 37˚C for 5 minutes and 21˚C for 10 minutes. The ligation reactions were then treated with PlasmidSafe exonuclease, 10X PlasmidSafe buffer and 10 mM ATP, at 37˚C for 30 minutes followed by 70˚C for 30 minutes to digest residual linearized DNA. Next the ligated products were transformed into 50 µl Subcloning Efficiency

DH5α competent cells (ThermoFisher Scientific) using heat shock. Ten percent of the total volume of bacteria was used to spread onto Luria Broth (LB) plates containing ampicillin and incubated overnight at 37˚C. Three bacterial colonies were randomly selected from each plate for each sgRNA design and inoculated into 3 ml LB medium along with 100 µg/ml ampicillin. The liquid cultures were shaken at 37˚C at 250 rpm overnight. Plasmids were extracted the following day using PureLink™ Quick Plasmid Miniprep Kit (ThermoFisher Scientific). The sequence of each colony was verified by Retrogen sequencing using the U6-Forward primer.

For large-scale isolation of plasmid DNA, sequence-verified sgRNA-Cas9 plasmids were transformed into µl Subcloning Efficiency DH5α competent cells (ThermoFisher Scientific) using heat shock. Bacteria was spread onto LB plates with ampicillin and incubated overnight at 37˚C. Single bacterial colonies were then selected to inoculate 3 ml of LB medium with 100 µg/ml ampicillin and incubated at 37˚C and 250 rpm. Following 8 hours of incubation the subsequent growth of the bacteria (starter culture) was then used to inoculate 50 ml of LB medium with 100 µg/ml ampicillin and shaken at 37˚C and 280 rpm overnight to increase the volume of bacteria cultured. Plasmids were then extracted the next day using the Qiagen Plasmid Midi Kit.

2.3 Restriction Enzyme Digestion of sgRNA-Cas9 Constructs

To further verify positive insertion of annealed sgRNA oligos and plasmid construct, sgRNA-Cas9 expression constructs were digested with FastDigest Bpil (BbsI) or FastDigest BglII (ThermoFisher Scientific) according to manufacturer's instructions. The digestion reaction composed of 1 µl 10X FastDigest Green Buffer, 200 ng of plasmid DNA, 0.5 µl FastDigest enzyme, and nuclease-free water to a total reaction volume of 10 µl. The reaction mixture was

incubated at 37˚C in a heat block for 25 minutes. Following digestion, the mixture was loaded onto 1% agarose gel and ran for 1 hour at 100 V.

2.4 PCR Amplification and Isolation of Venus_p2a_Neo from Donor Plasmid

The 4263 bp donor plasmid containing the Venus_p2a_Neo sequence was provided by the Stewart-Ornstein and Lahav lab. Primers with flanking homology arms were used to amplify the Venus_p2a_Neo sequence using PCR. The primer sequences are shown in Table 2.1. The PCR were performed with Herculase II Fusion DNA Polymerase (Agilent) with the following thermocycling protocol: (1) initial denaturation at 95˚C for 2 minutes, (2) 33 cycles of 3-step amplification (95˚C for 20 seconds, 72˚C for 20 seconds, 72˚C for 54 seconds), and (3) final extension at 72˚C for 3 minutes. Venus_p2a_Neo PCR products were run on 2% agarose gels for 45 minutes at 100 V. PureLink Quick Gel Extraction Kit (ThermoFisher Scientific) was used to isolate the Venus_p2a_Neo cassette for transfection.

Table 2.1 Sequence of Primers Used to Amplify Venus_p2a_Neo from Donor Plasmid. Homology arm sequences are underlined.

	Primer Sequence
Forward	ACGACGCGGACGCGCCTGCGGCCCGGGGAGCAGCAGCAGCCACAGCCACAGCAGCCGCCAGGAGCTGGTGCAGGCGCTGGAGCCGGTGCC
Reverse	GGCTCGCGGCGAGAGGCGCCGCCGACGACGACACCGACAGCGACGACGACGGCGAGATTTACCCACCTCCGCCAAGTAGTCTTCTTGAG

2.5 Human Cell Lines

HCT116 cells were maintained in in McCoy's 5A (modified) Medium supplemented with 1X Penicillin/Streptomycin (P/S) and 10% Fetal Bovine Serum (FBS). Cells were cultured at 37˚C and 5% CO2.

2.6 Transfection by Lipofectamine

HCT116 cells were seeded 24 hours prior to transfection and were transfected using Lipofectamine 3000 (ThermoFisher Scientific), following the company's protocol. Per 24-well plate transfection, 50 µl transfection mixture was used which contained: (1) 500 ng DNA, (2) 1 µl P3000 Reagent, and (3) 1.5 µl Lipofectamine 3000 Reagent diluted in Opti-MEM Medium. Per 6-well plate transfection, 250 µl transfection mixture was used which contained: (1) 2500 ng DNA, (2) 5 µl P3000 Reagent, and (3) 7.5 µl Lipofectamine 3000 Reagent diluted in Opti-MEM Medium. Puromycin selection of transfected cells was applied at a concentration of 3 µg/ml for 48 hours. Geneticin (G418) selection was used for 6 days, at a concentration of 500 µg/ml, following Puromycin selection for cells transfected with Venus_p2a_Neo cassette (ThermoFisher).

2.7 HCT116 Single Cell Cloning

Vector-transfected and pSpCas9(sgRNA)-transfected HCT116 cells were harvested from 24-well plates by trypsinization using 0.25% trypsin-EDTA. The TC20 Automated Cell Counter (Bio-Rad) was used to count viable cells. To generate single cell clones, each cell suspension was diluted to 1 cell/600 µl. 200 µl of this suspension was used to seed 96-well plates.

2.8 Genomic DNA Extraction by QuickExtract and Genomic PCR

In order to extract genomic DNA from cells growing in 96-well plates, cells were washed with 200 µl phosphate-buffered saline (PBS) and 10 µl of QuickExtract^{TM} DNA Extraction Solution (Lucigen) was added per well. Plates were tapped against a hard surface at each of the four sides to evenly spread the solution across the wells. Plates were then wrapped in aluminum

foil and incubated on a hot plate at 70˚C for 6 minutes. Following this incubation, plates were tapped again for 15 seconds on each side and incubate at 100˚C for 5 minutes. 1 µl of solution was used for each genomic PCR reaction. PCRs were performed using Taq DNA Polymerase (NEB) with the following thermocycling conditions: (1) initial denaturation at 95˚C for 30 seconds, (2) 33 cycles of 3-step amplification (95˚C for 20 seconds, primer specific annealing temperature (Ta) ˚C for 20 seconds, 68˚C for 20 seconds), and (3) final extension at 68˚C for 5 minutes. Genomic PCR products were run on 2% agarose gels for 45 minutes at 100 V.

2.9 TOPO Cloning and Sequencing for Insert

Fresh genomic PCR products were incubated at room temperature for 5 minutes with TOPO vector from the TOPO TA Cloning Kits for Sequencing (Invitrogen) at a 4:1 ratio. 1 µl of the TOPO cloning reaction was transformed into MAX Efficiency™ DH5α-T1 Competent Cells using heat shock. Bacteria was then spread onto LB-ampicillin plates that were pre-added with 40 µl of 40 mg/ml X-gal. Plates were incubated at 37˚C. Eight light blue colonies were randomly selected per reaction for plasmid extraction using PureLink™ Quick Plasmid Miniprep Kit (Invitrogen). The nucleotide sequences of the genomic PCR products were obtained by Sanger Sequencing (Retrogen) using the M13 Forward (-20) primer.

2.10 Immunoblotting

In preparation for WCL harvesting, cells were removed from 37˚C and 5% CO2 incubation and place into ice. The cell media was collected, and each well was washed with ice-cold 1X PBS and also transferred into a 15-ml Falcon tube. Cell suspension was centrifuged at 800 rpm for 5 minutes at 4˚C. Supernatant was removed and cells were resuspended in 1 ml of

ice-cold 1X PBS and transferred into 1.5 ml Eppendorf tubes. Cell suspension was centrifuged again using the Eppendorf 5415 Centrifuge at max speed for 10 seconds. Supernatant was removed and cell pellets were lysed in RIPA buffer (ThermoFisher Scientific) with Protease Inhibitor Cocktail (Sigma) and phenylmethanesulfonyl fluoride mixtures for 20 minutes on ice. Lysed cells were then subjected to 10 pulses of sonication with the following settings: (1) MicroTip 3, (2) Pulse 50, (3) Hold. Following sonication, the lysed solution was centrifuged at 14,000 rpm for 30 minutes at 4˚C. Protein concentration was measured using Bio-Rad DC Protein Assay. Total cell lysates were separated by SDS-PAGE gel electrophoresis on 4-15% Min-PROTEAN TGX Precast Protein Gels (Bio-Rad) and proteins were transferred from mini or midi gels to polyvinylidene fluoride (PVDF) membranes (Bio-Rad) using the Mini TGX or MIXED MW program of the Trans-Blot Turbo Transfer System (Bio-Rad) for mini and midi gels respectively. Blots were blocked with 5% nonfat dry milk in 1X TBST (Tris-buffered saline with 0.1% Tween 20) for 1 hour and incubated with primary antibodies against PUMA-α (Pro-Sci; 3043), PUMA-α/β (Santa Cruz Biotechnology; sc-374223), p53 (Santa Cruz Biotechnology; FL-393), p21CIP1 (Millipore Sigma; EA10), GAPDH (Cell Signaling Technology; 2118S), c-MYC, PARP (Cell Signaling Technology; 46D11), Caspase-3 (Cell Signaling Technology; 8G10), Phospho-Histone H2A.X (Cell Signaling Technology; 20E3), and Neo (Millipore; 06-747) at a concentration of 1 μg/ml. Blots were washed in 1X TBST three times for 5 minutes and incubated with horseradish peroxidase (HRP)-conjugated rabbit or mouse secondary antibodies (Cell Signaling Technology) for 1 hour at room temperature. Blots were washed again in 1X TBST three times for 5 minutes and developed using SuperSignal West Pico PLUS Chemiluminescent Substrate (ThermoFisher Scientific), according to manufacturer's instructions. Blot imaging was performed using ChemiDoc MP imager (Bio-Rad)

2.11 Treatment with 4EGI-1 and 5-FU Separately or in Combination

HCT116 cells were seeded on 6-well plates at 600,000 cells/wells 24 hours prior to the pre-treatment stage. During the pre-treatment stage, cells were treated with either DMSO or 50/100 μM 4EGI-1 for 4 hours (Figure 4.11). At the end of the 4-hour pre-treatment, DMSO or 385 μM 5-FU was added and cells were incubated for an additional 12 hours (Figure 4.11). The final concentration of DMSO for each treatment is 0.2%. Following 16 hours since drug treatment, cells were harvested for whole cell lysate (WCL) and RNA preparation (Figure 4.11).

2.12 RNA Extraction, cDNA Synthesis, and qRT-PCR

Drug treated cells were harvested for RNA extraction using the RNeasy Mini Kit (Qiagen) according to the manufacturer's protocol. RNA concentration was measured using NanoDrop and RNA integrity (distinct 28S and 18S band with the intensity of the 28S being twice that of the 18S band) was checked using RNA Gel Electrophoresis. 1000 ng of RNA was run on a 1% agarose gel containing 0.5 μg/ml EtBr for 60 minutes at 80 V. 1 μg of RNA was used per cDNA synthesis reaction using the ProtoScript II Reverse Transcriptase (NEB) according to manufacturer's instructions. 5% of the cDNA synthesis reaction was used as the template for qRT-PCR. SYBR Green PCR Master Mix (ThermoFisher Scientific) was used to measure amplification of PCR products. Specific exon-exon spanning primers were designed to measure specific mRNA abundance (Table 2.2). The qRT-PCR was run in the QuantStudio Real-Time PCR System (ThermoFisher Scientific).

Table 2.2 Primer Pair Sequences for qRT-PCR Quantification.

qRT-PCR Primers	Forward	Reverse	Product size (bp)	Tm (C)
p53	CCTCAGCATCTTATCCGAGTGG	TGGATGGTGGTACAGTCAGAGC	128	58
p21	CTGGAGACTCTCAGGGTCGAAA	GATTAGGGCTTCCTCTTGGAGAA	97	58
PUMA	CTCAACGCACAGTACGAGC	TGATGAGATTGTACAGGACCCTC	85	58
MYC	CCTGGTGCTCCATGAGGAGAC	CAGACTCTGACCTTTTGCCAGG	128	58
GAPDH	GTCTCCTCTGACTTCAACAGCG	ACCACCCTGTTGCTGTAGCCAA	131	58

2.13 References

Stewart-Ornstein, J., Lahav, G. (2016). Dynamics of CDKN1A in Single Cells Defined by an Endogenous Fluorescent Tagging Toolkit. *Cell Reports, 14,* 1800-1811. doi: 10.1016/j.celrep.2016.01.045

Ran, F. A., Hsu, P. D., Wright, J., Agarwala, V., Scott, D. A., & Zhang, F. (2013). Genome engineering using the CRISPR-Cas9 system. *Nature protocols*, *8*(11), 2281–2308. https://doi.org/10.1038/nprot.2013.143

CHAPTER 3 EDITING THE *BBC3* EXON-4 ALLELES TO DELETE C-TERMINAL CODING SEQUENCES OF PUMA-α

3.1 Goal of this Editing Project

Prior to conducting immunoblotting experiments with commercial antibodies, it is important to verify their authenticity and ascertain that they indeed detect the specified proteins. The goal of this editing project is to verify two commercial antibodies: anti-PUMA-α (ProSci) and anti-PUMA-α/β (Santa Cruz Biotechnology) for reactivity with the endogenous human PUMA-α protein. I used the CRISPR/Cas9-double cutting strategy to remove 54 base pairs (bp) of coding sequence from Exon-4 of the *BBC3* gene including the translation termination codon of the PUMA-α ORF. Following non-homologous end joining (NHEJ) repair pathway, I expect the edited *ΔBBC3* alleles to produce PUMA-α with alterations in the C-terminal 18 amino acids, depending on how the two CAS-9-but sites are re-joined by NHEJ. If the two commercial antibodies are specific to binding PUMA proteins, I expect the antibodies to detect PUMA-α proteins with altered sizes, consistent with sizes by the sequence alterations, in the Δ*BBC3*-edited clones.

3.2 Designing sgRNAs for the Double-Cutting Strategy

Two sgRNAs were selected to edit the C-terminal amino acids of based on their target sites, on-target efficacy scores, and off-target rankings from the Broad Institute (https://portals.br oadinstitute.org/gpp/public/analysis-tools/sgrna-design) (Figure 3.1). The sgRNA is named by the oligonucleotides used for cloning, e.g., sgRNA 11/12 denotes the sgRNA coding fragment annealed from oligonucleotides 11 and 12 and has an on-target efficacy score of 0.4131 and an off-target rank of 166 (Figure 3.1). When expressed as a CRISPR with

the Cas9-binding scaffold RNA, sgRNA 11/12 guides Cas9 nuclease to make a cut 30 bp upstream of the PUMA-α stop codon. On the other hand, sgRNA 3/4 has an on-target efficacy score of 0.6567, an off-target rank of 8 and guides Cas9 nuclease to make a cut 16 bp downstream of the PUMA-α stop codon. Based on the numerical values of the on-target efficacy scores and off-target ranks, sgRNA 3/4 is more specific and less likely to result in off-target cleavage than sgRNA 11/12, because sgRNA 3/4 has a higher efficacy score and lower off-target ranking when compared to sgRNA 11/12. Another factor that was taken into consideration when selecting these two sgRNAs is the orientation of the PAM sequences that dictate the CAS9 cut sites (Figure 3.1). In this design, the two sgRNAs target opposite DNA strands in a PAM-out orientation that is more favorable for double-cutting as it results in higher editing compared to the "PAM-in" orientation configuration (Bothmer et al., 2017).

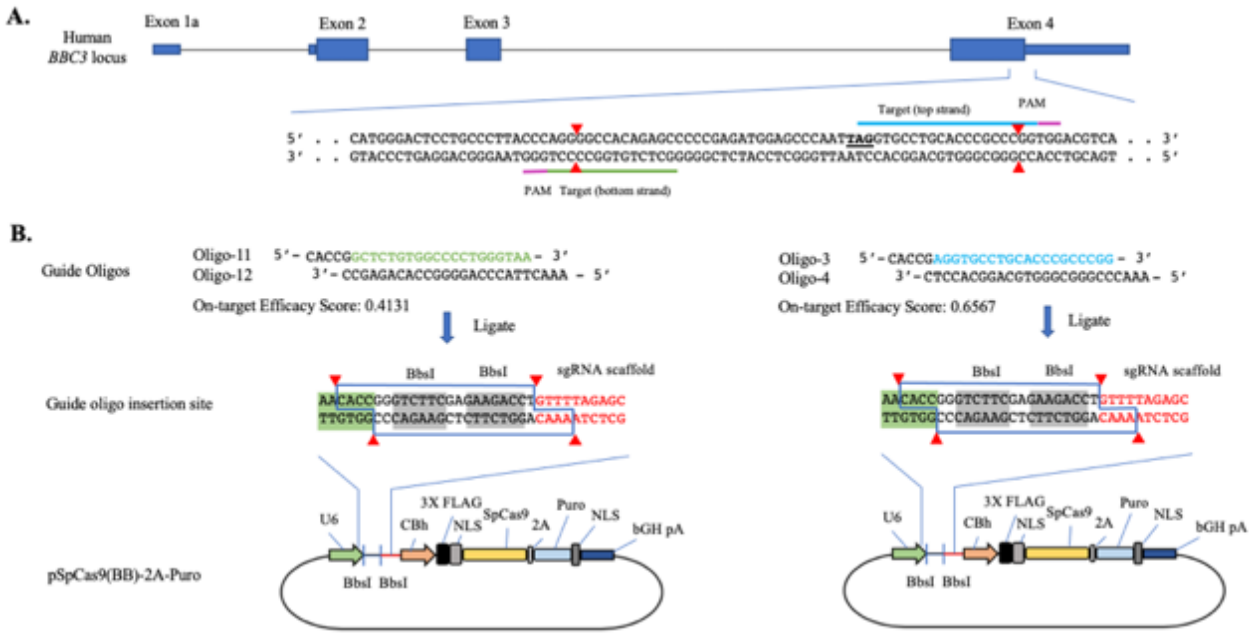

Figure 3.1 Selection of Two sgRNAs for Deleting the C-terminal Amino Acids of PUMA-α by Double-Cutting. (A) The sgRNA targets and the CAS9 cut sites in Exon-4 of the PUMA-α mRNA on either side of the translation termination codon (TAG, bold and underlined). The two sgRNAs are oriented in the PAM-out orientation to facilitate double-cutting. (B) Construction of the targeting plasmids in the pSpCas9(BB)-2A-Puro vector. The sgRNAs (corresponding to Oligo-11 and Oligo-3) were selected from the list of *BBC3*-targeting guide-RNAs at the Broad Institute GPP sgRNA Designer website for their on-target efficacy scores and their targeted cut sites relative to the termination codon. The sgRNA- oligo insertion site is between the U6 promoter and the CRISPR RNA scaffold sequence in the vector. The restriction enzyme BbsI is used to digest the vector plasmid, between nucleotides indicated by the red triangles, to replace the BbsI restriction sites (blue outline) with the annealed oligos. Nucleotides highlighted in grey are the BbsI recognition sites. The components of the pSpCas9(BB)-2A-Puro are shown as CBh: chicken β-actin promoter with hybrid intron; 3X FLAG: 3 tandem FLAG epitope tags (DYKDHD-G-DYKDHD-I-DYKDDDDK); NLS: nuclear localization signal from the SV-40 viral large T-antigen; 2A: the self-cleaving 2A peptide from Thosea asigna virus capsid protein; Puro: puromycin resistance gene; bGHpA: bovine growth hormone polyadenylation signal.

3.3 Construction of sgRNA-Expressing Plasmids

Each guide oligo (Oligo-11, 12, 3, 4) were annealed to their pair to form annealed sgRNA oligos 11/12 and 3/4. These annealed oligos were then ligated into pSpCas9(BB)-2A-Puro following digestion of the plasmid with BbsI which removed the restriction sites and allowed for the direct insertion of the annealed sgRNA oligos (Figure 3.1) between the U6 promoter and the CRISPR scaffold sequence. In summary, the sgRNA 11/12 and sgRNA 3/4 were each cloned into the pSpCas9(BB)-2A-Puro to form sgRNA-expressing plasmids. Each sgRNA-expressing plasmid construct was transformed into Subcloning Efficiency DH5α competent cells (ThermoFisher Scientific) and transformed cells were grown on LB-Ampicillin plates. For each transformation three randomly picked bacterial colonies were selected for plasmid extraction and were verified by restriction enzyme digestion with BbsI. Successful insertion of the sgRNA oligos into the pSpCas9(BB)-2A-Puro vector destroys the BbsI recognition sites. Therefore pSpCas9(BB)-2A-Puro vector with the correct annealed sgRNA oligo insert cannot be digested by BbsI into linear DNA. The restriction digestion verified plasmids were further verified by Sanger sequencing (Retrogen) to confirm that the sgRNA oligo insertions have the correct nucleotide sequence.

Larger quantities of DNA for each sgRNA-expressing plasmid were also generated in preparation for transfection using midiprep. BbsI digestion and Sanger sequencing were used again to verify successful insertion of the sgRNA oligos and correct nucleotide sequences. BglII digestion was also performed to verify the size of linearized sgRNA-expressing plasmid constructs. The expected linear size of the pSpCas9(BB)-2A-Puro plasmid is ~ 9000 base pairs. Both the sgRNA-11/12 and sgRNA-3/4 constructs was able to be linearized by BglII with band sizes corresponding to 9000 bp on gel electrophoresis.

3.4 Isolating *ΔBBC3* Edited Single Clones

HCT116 cells were transfected with both the sgRNA-11/12 and sgRNA-3/4 plasmids by lipofectamine to introduce two double stranded cuts at the C-terminus of the *PUMA-α* ORF in Exon-4. A mock transfection, in which no plasmid DNA was added, and a vector control transfection, using pSpCas9(BB)-2A-Puro without sgRNA insert, were included to serve as the negative and positive controls respectively. At 24 hours post transfection, cells were split into two puromycin containing media for 48 hours to select for transfected cells. The sgRNA-11/12-3/4 transfected cells and vector control transfected cells were expected to survive the puromycin treatment because they obtained puromycin resistance from the pSpCas9(BB)-2A-Puro vector. After 48 hours of puromycin selection, when all mock-transfected cells died, I collected the sgRNAs and vector transfected cells and seeded them at low density in 96-well plates to obtain single clones. Single clone expansion was monitored daily and when colonies that formed from single cells became 30% confluent, they were collected for genomic PCR screening and propagation. Genomic DNA was extracted from each potential clone and genomic PCR primers, that flanked the edited region of Exon-4, were used to screen for *ΔBBC3*-edited clones (Table 3.1 & Figure 3.1A). The expected length of the genomic PCR products from wild-type *BBC3* is 204 bp while the expected length of the *ΔBBC3* is 150 bp. The genomic PCR products were separated by gel electrophoresis to identify clones that had either wild-type or edited band size. Figure 3.1B is a representative gel electrophoresis image that depicts the genomic PCR products from 20 sgRNA-11/12 and -3/4 transfected HCT116 clones. The absence of bands in the water control lane in Figure 3.1B indicates that there were no gDNA contamination in the PCR reactions. Based on the screening results, clones F3, F9, and F18 each had one band at 150 bp. The remaining clones either had a single band at 204 bp, double band at 204 bp and 150 bp, or

multiple bands of varying sizes. Clones with multiple varying band sizes suggest that the homologous recombination for each of their *BBC3* allele is heterozygous. Only homozygous *ΔBBC3*-edited clones (F3, F9, and F18) were selected for further expansion and sequencing. These three clones were then renamed as *BBC3*-Δ7, -Δ25**,** -Δ37 respectively.

Table 3.1 Sequence of Genomic PCR Primers Used to Screen for Δ*BBC3*-Edited Clones.

	Primer Sequence
Forward	CCTGGAGGGTCCTGTACAATC
Reverse	AGGGCTGGGAGTCCAGTATG

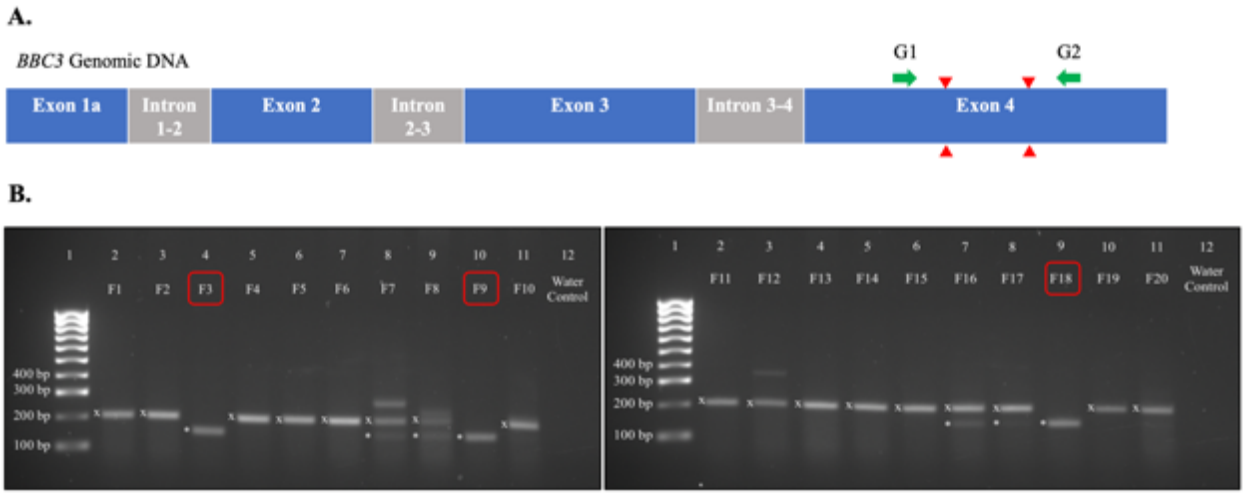

Figure 3.2 Identifying Δ*BBC3*-Edited Clones by Genomic PCR. (A) Positions of genomic primers for screening desired Δ*BBC3* clones. The forward primer (G1) is 23 base pairs upstream of the sgRNA 11/12 cut site (left red triangles) and the reverse primer (G2) is 86 base pairs downstream the sgRNA 3/4 cut site (right red triangles). The expected PCR product of wild-type *BBC3* and *ΔBBC3* is 204 and 150 bp respectively. (B) Genomic PCR fragments from single cell clones following co-transfection with the sgRNA-11/12 and sgRNA-3/4 targeting plasmids. Bands marked with * are the same bp length as the expected *ΔBBC3* PCR product. Bands marked with X are the same bp length as the wild-type *BBC3* PCR product. Three potential clones (boxed in red) were selected for expansion and sequencing.

3.5 Predicted Protein Products from the *ΔBBBC3*-Edited Clones

To determine the nucleotide sequences of *BBC3*-edited clones-Δ7, Δ25, Δ37, the genomic PCR fragments for each clone were cloned into the TOPO vector and transformed into chemically competent bacteria. Light blue colonies, on LB Ampicillin and X-Gal plates, were selected for PCR-TOPO plasmid extraction and sequencing. The genomic fragment sequences for each of the *BBC3*-edited clones are shown in Figure 3.3A. Alignment of the genomic PCR fragment sequences of the *ΔBBBC3* clones to wild-type *BBC3* gene revealed that Cas9 cutting can result in different deletion outcomes. The *ΔBBBC3*-edited clones 7 and 37 (Δ7 and Δ37) lost 53- and 54- nucleotides respectively as a result of double-cutting and non-homologous end-joining. Clone 25 (Δ25) appeared to result from cutting at the sgRNA 3/4 targeted site only followed by indel formation to lose 58-nucleotides (Figure 3.3A).

From the nucleotide sequences, I predicted the amino acids alterations to the C-terminal region of PUMA-α from each of these three *ΔBBC3*-edited clones (Figure 3.3B). The wild-type PUMA-α protein is composed of 193 amino acids with a molecular weight of 24 kDa. The PUMA-α protein produced by the *ΔBBBC3*-allele in clone Δ7 is expected to be 16 aa longer and have a molecular weight of 26 kDa (Figure 3.3B). Even though clone Δ25 had the largest number of deleted nucleotides the resulting change of the PUMA-α ORF for this clone only differed by two amino acids compared to wild-type PUMA-α with a predicted molecular weight of 24.1 kDa (Figure 3.3B). Clone Δ37 is expected to produce PUMA-α protein that is 43 aa longer with a predicted molecular weight of 29 kDa.

3.6 Verification of Commercial Anti-PUMA Antibodies by Reactivities to PUMA-α from *ΔBBC3*-Edited Clones

To induce the expression of PUMA-α, I used a DNA damaging agent 5-fluorouracil (5-FU). 5-FU is used in the clinic to treat cancers including breast and colorectal cancers (Wigmore et al., 2010). This drug inhibits the enzyme thymidylate synthase which blocks the thymidine formation required for DNA synthesis. Previous studies have shown that 5-FU induces PUMA-α mRNA and protein in HCT116, a p53-proficient colon cancer cell line (Yu et al., 2001). The parental HCT116 cells, the three Δ*BBC3*-edited clones and two control clones isolated from vector-transfected HCT116 cells were treated with vehicle (DMSO) or 5-fluorouracil (5-FU) for 24 hours and whole cell lysates (WCL) were then prepared and analyzed by western blotting using two commercial antibodies that detected PUMA-α or PUMA-α/β (Figure 3.4A, B). By blotting with anti-GAPDH, I detected GAPDH protein bands with the expected MW of 37 kDa in each sample at approximately similar intensity (Figure 3.4B). This indicates that equal amounts of proteins were loaded across samples. The anti-PUMA-α antibody only reacts with PUMA-α isoform but does not react with PUMA-β, γ, or δ, as this antibody was raised against PUMA-α specific amino acids 1-50 (Figure 3.4A). On the other hand, the epitope target of anti-PUMA-α/β antibody is located in amino acids 57-193 that are commonly found in both PUMA-α and PUMA-β proteins (Figure 3.4A). When reacted with WCLs from HCT116 cells and control clones, both anti-PUMA-α and anti-PUMA-α/β detected the wild-type PUMA-α protein with the expected molecular weight (~24 kDa), and the expected increases in 5-FU treated cells (Figure 3.4B, lanes 1, 2). Furthermore, the two antibodies detected identical bands showing that HCT116 cells express the PUMA-α isoform. In the three Δ*BBC3*-edited clones examined, both antibodies again detected bands of identical patterns and sizes, confirming that the Δ*BBC3*-edited clones

also expressed the PUMA-α isoforms, and that both antibodies specifically reacted with PUMA protein. In Clone ΔC7 (Figure 3.4B, lanes 3, 4), a 5-FU-induced band of ~ 26 kDa was detected, which migrated slower than the band of ~24 kDa in the parental (P) (Figure 3.4B, lanes 1, 2) and the control clones (cC1, cC2) (Figure 3.4B, lanes 9-12). In Clone Δ37, a band of ~29 kDa was reactive to both anti-PUMA antibodies and induced by 5-FU treatment (Figure 3.4B, lanes 7, 8). These two higher MW PUMA-α proteins in ΔC7 and ΔC37 migrated on SDS-PAGE at the predicted MWs (Figure 3.3B) and reacted with both antibodies, and therefore, are likely to be encoded by the Δ*BBC3*-alleles in these edited clones. In Δ25, a, band of ~24 kDa and a band of ~28 kDa were found to react with the two anti-PUMA antibodies (Figure 3.4B, lanes 5, 6). The predicted size of the C-terminal modified PUMA-α from this edited clone is ~24 kDa (Figure 3.3B). The origin of the ~28 kDa band, which reacted with both anti-PUMA antibodies and was induced by 5-FU is likely to be encoded by another Δ*BBC3*-edited allele that was missed in the sequencing experiment. Nevertheless, the results in Figure 3.4B confirmed that the two commercial anti-PUMA antibodies can detect wild-type and C-terminal-modified PUMA-α proteins expressed at basal and 5-FU induced levels from the endogenous *BBC3* gene in human cells.

3.7 DNA-Damage-Induced Cell Death is Reduced in Δ*BBC3*-Edited Clones

The C-terminal region of PUMA-α contains a transmembrane domain that mediates the insertion of PUMA-α into the mitochondrial outer-membrane (Andreu-Fernandez et al., 2016). Previous study has found that recombinant PUMA-α proteins with C-terminal deletions show defects in the activation of mitochondria-dependent intrinsic apoptosis (Andreu-Fernandez et al., 2016; Yee & Vousden, 2008). Although the Δ*BBC3*-edited alleles retain the coding sequence for

the core membrane-insertion alpha helix, RPSPWRVLYNLIMGLLPLPRGHR, the editing does alter the amino acids that are C-terminal to this membrane insertion helix. I therefore determined whether these C-terminal modifications of PUMA-α could affect the cell death response to DNA damage.

To compare the DNA damage response pathway among the parental and clones of HCT116 cells, I measured the levels of p53, p21CIP1, and γ-H2AX in whole lysates of cells treated with vehicle (DMSO) or 5-FU (Figure 3.4fB). It is well established that DNA damage activates PIKKs (ATM, ATR, and DNA-PK) to phosphorylate histone H2AX at Serine-139 (Jackson et al., 2009; Fagagna, 2008). The phosphorylated H2AX is named γ-H2AX, and its levels can be measured by a phosphor-specific antibody and is widely used as a surrogate marker for double-stranded breaks (Yuan et al., 2010). The PIKKs also phosphorylate stabilized, and activate p53, which then stimulates the transcription of CDKN1 (which encodes p21CIP1) and *BBC3* (which encodes PUMA-α). As shown in Figure 3.4B, 5-FU induced similar increases in the levels of p53 and p21CIP1 in the parental and the clones of HCT116 cells, showing that modifications of the C-terminal region of PUMA-α did not affect DNA damage signaling though p53 to p21CIP1. Interestingly, 5-FU induced γ-H2AX increases were less robust in ΔC7 and ΔC37, compared to parental, ΔC25, and control clones. Because γ-H2AX levels measure the levels of double-stranded breaks (DSBs) in DNA, and because executioner caspases activated in the intrinsic apoptosis pathway cleave genomic DNA to generate DSBs, γ-H2AX could result from 5-FU-induced DSBs and caspase-induced DSBs. Since 5-FU induced p53 and p21CIP1 was not reduced in Δ7 and Δ37 clones, the reduction in γ-H2AX these two clones could indicate reduced caspase activities.

To assess the cellular levels of executioner caspase activities, I probed whole cell lysates (WCL) with anti-PARP1 and anti-pro-caspase 3 (Figure 3.4B). PARP1 is a highly abundant nuclear poly-ADP ribose polymerase of 116 kDa that is cleaved by executioner caspases at a single cleavage site to generate a cleaved PARP1 (ΔPAPR1) of 89 kDa (Fernandes-Alnemri et al., 1994). Thus, the fraction of ΔPAPR1 in WCL, therefore, can reflect the activity of executioner caspases in the nucleus. Caspase-3 is one of three executioner caspases that are activated by the initiator caspase-9-mediated cleavage of an inactive pro-caspase-3 in the intrinsic apoptosis pathway (Nicholson et al., 1995). Thus, the cleavage of pro-caspase-3 can reflect the activity of the initiator caspase-9 in the cytoplasm. In my experiments, I probed WCL with an anti-pro-caspase-3 that reacts with the full-length, uncleaved caspase-3; therefore, cleavage by caspase-9 would result in reduction of the full-length pro-caspase-3 band. As shown in Figure 3.4B, 5-FU induced the cleavage of PARP1 and the reduction in pro-caspase-3 to varying degrees in the parental and clones of HCT116 cells. Overall, the extent of PARP1 cleavage and loss of full-length caspase-3 is correlated, showing that 5-FU activated intrinsic apoptosis to different levels among the cells examined.

To quantify PARP1 cleavage, I determined the fraction of ΔPARP1 by densitometry scanning of two anti-PARP1 blots. I first normalized the band intensity of PARP1 and ΔPAPR1 in each lane relative to that of GAPDH, and then calculated *f*ΔPARP1 as the normalized ΔPARP1 density/sum of the normalized densities of PARP1+ΔPARP1 (Figure 3.5A). To determine whether C-terminal modifications of PUMA-α consistently affected 5-FU-induced cleavage of PARP1, I calculated the mean±SD of *f*ΔPARP1 from the three Δ*BBC3*-edited clones as one cohort, and the mean±SD of *f*ΔPARP1 from the parental and the two control clones as another cohort. As shown in Figure 3.5B, this cohort analysis of 5-FU induced PARP1 cleavage

showed a significant difference (p = 0.0128768) between cells expressing the wild-type versus the C-terminal modified PUMA-α and suggesting that modifications of the C-terminal amino acids could indeed reduce the pro-apoptotic activity of PUMA-α.

To directly quantify the cell death response to 5-FU, the parental, the *ΔBBC3*-edited, and the control clones were treated with 5-FU for 24 hours and cell death was measured by trypane blue counting where dead cells are stained blue. As shown in Figure 3.6A, the Δ*BBC3*-edited clones showed lower levels of cell death than the parental and the control clones. The cohort analysis, where I calculated the mean±SD of cell death percentage from parental and control clone and that from the three Δ*BBC3*-clones showed that cells expressing wild-type PUMA-α had a death percentage of 33.2 ± 6.7 which was significantly higher (p = 7.48E-10) than the death percentage of 15.6 ± 5.8 in cells expressing C-terminal modified PUMA-α (Figure 3.6B). Together, results from Figures 3.4, 3.5, and 3.6 demonstrate that C-terminal modifications of the endogenous PUMA-α protein can indeed interfere with its pro-apoptotic activity.

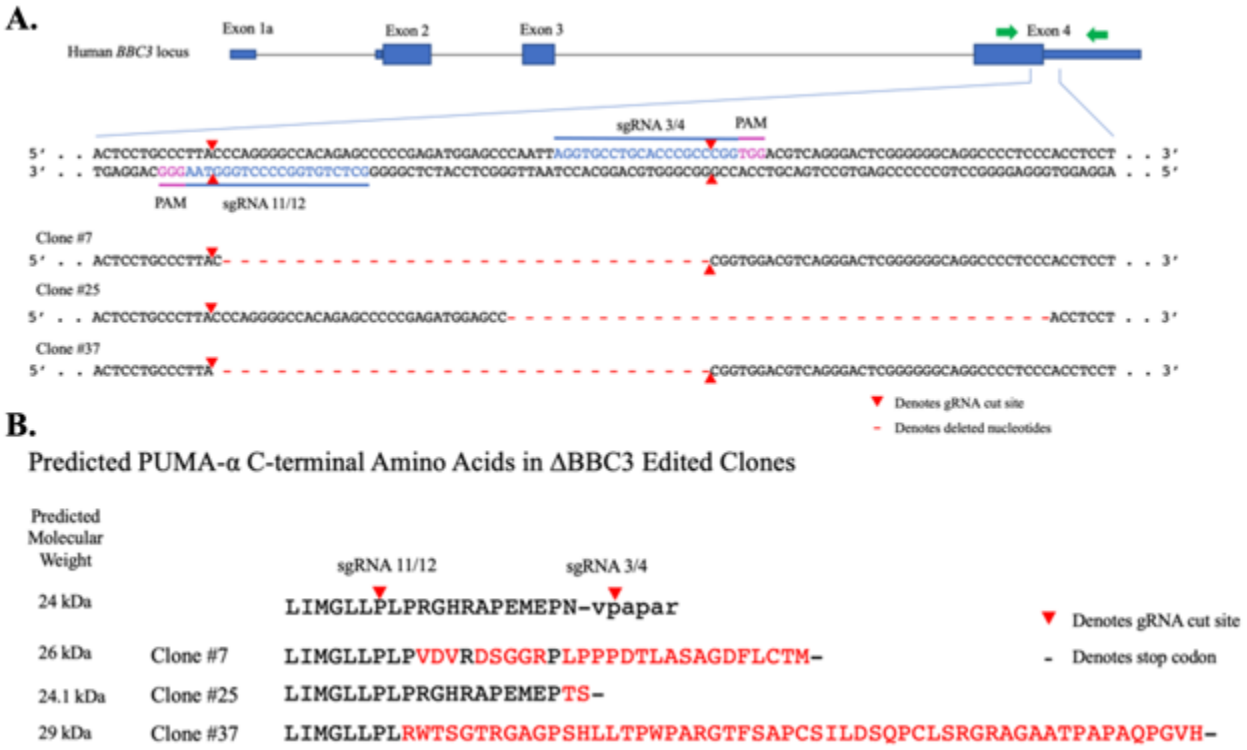

Figure 3.3 Nucleotide and Predicted Amino Acid Sequences in Edited Δ*BBC3* Clones. (A) Nucleotides deleted in three Δ*BBC3* clones analyzed. The sgRNA target sites and the PCR primers (denoted in green) used to amplify genomic fragments from the edited clones for sequencing are shown. The PCR fragments amplified by the PCR primers using genomic DNA of wild-type *BBC3* is 204 bp in length. The Δ*BBC3* clones 7 and 37 lost 53- or 54-nucleotides, respectively, as a result of double-cutting. The Δ*BBC3* clone 25 appeared to result from single-cutting at the sgRNA 3/4 targeted site followed by indel formation, leading to a 58-nucleotide deletion. (B) Predicted C-terminal amino acids in each of the three ΔBBC3 clones: The wild-type PUMA-α C-terminal amino acids are in black CAP letters. Amino acids beyond the termination codon (marked as -) are in small black letters. Predicted C-terminal amino acids that deviate from the wild-type in each of the three Δ*BBC3* clones are in red letters with predicted termination codon marked as (-). The predicted MWs of the modified PUMA-α proteins from the wild type, and each of the Δ*BBC3* clones are shown.

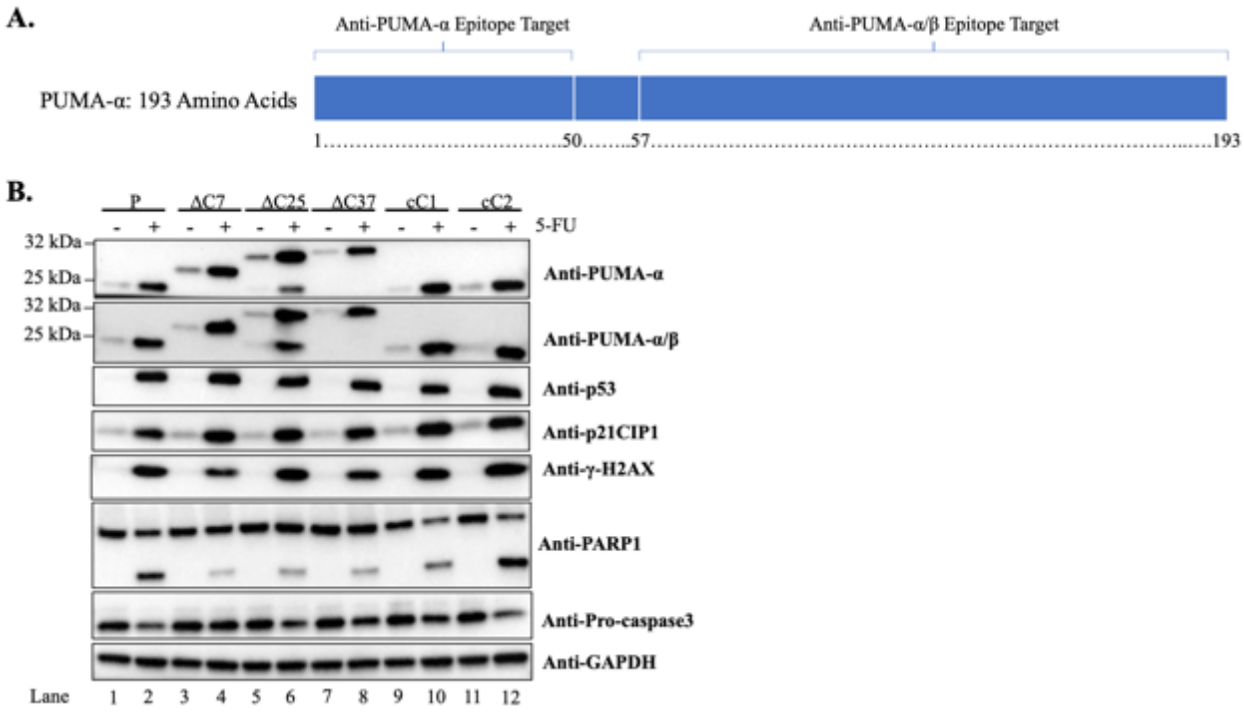

Figure 3.4 DNA Damage-Induced Expression of WT and Δ*BBC3* PUMA-α Proteins. (A) Location of epitopes for the anti-PUMA-α and the anti-PUMA- a/b antibodies in the PUMA-α protein. (B) The Parental HCT116 cells (P), three Δ*BBC3* clones (ΔC7, ΔC25, ΔC37) and two vector transfected control clones (cC1 & cC2) were treated with 0.1% DMSO (vehicle) or 385 μM 5-FU for 24 hours. Whole cell lysates were probed with the indicated antibodies to detect proteins in DNA damage response and caspase activation, with GAPDH as a loading control.

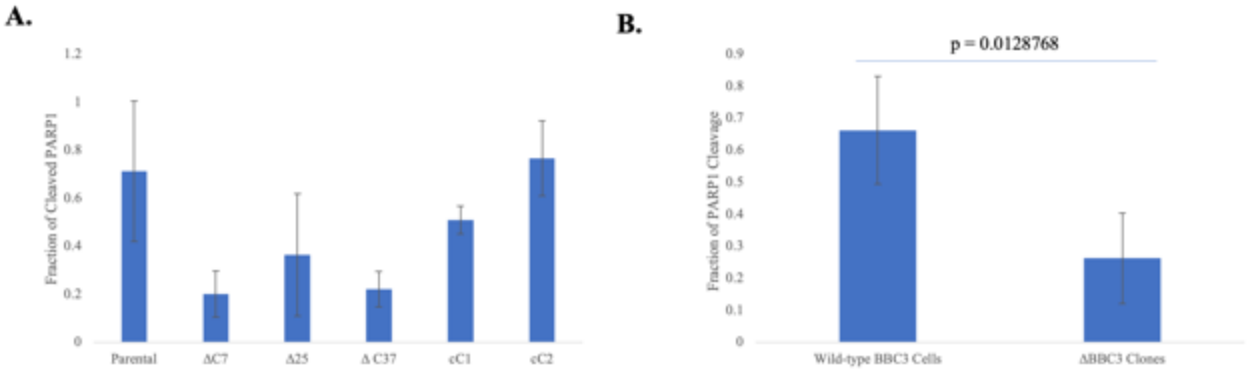

Figure 3.5 Extent of 5-FU-Induced PARP1 Cleavage. (A) The fraction of cleaved PARP1 was calculated from densitometry quantifications of two technical repeats. Western blots in the indicated cells as ΔPARP1/Full-length PARP1+ΔPARP1 in each indicated cell populations. (B) 5-FU-induced PARP1 cleavage in Δ*BBC3* clones (Δ7, Δ25, Δ37) was significantly lower than that in the parental HCTT116 cells and the vector-transfected clones (cC1 and cC2).

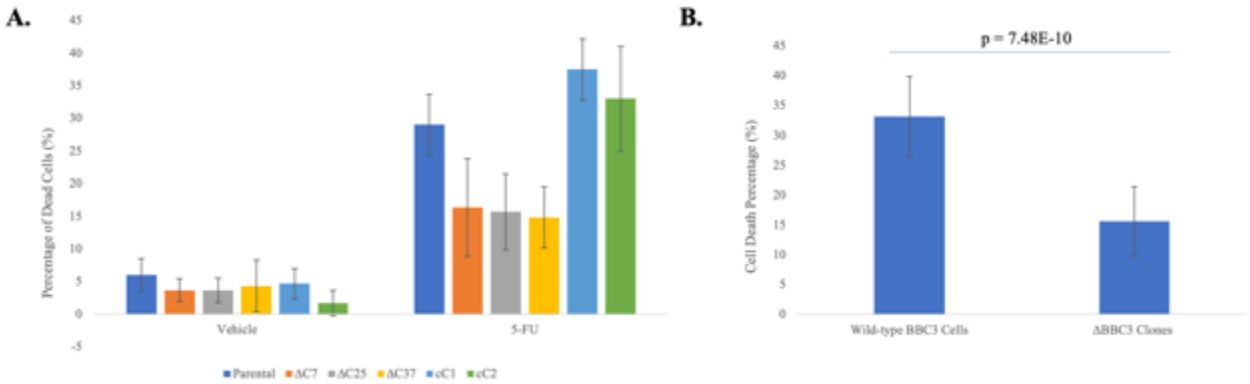

Figure 3.6 DNA Damage-Induced Cell Death is Reduced in Δ*BBC3* Clones. (A) The indicated HCT116 parental and single cell clones were treated with 0.1% DMSO (vehicle) or 385 μM 5-fluorouracil (5-FU) for 24 hours, and cell death measured immediately following trypsinization by trypane blue counting. The values shown are average of % trypane blue positive cells from two counting chambers per sample. (B) 5-FU-induced cell death from parental HCT116 cells and control clones was significantly higher than that from Δ*BBC3* clones (Δ7, Δ25, Δ37) . The average cell death percentage from wild-type *BBC3* cells (Parental, cC1, cC2) is 33.17 ± 6.67 at 24 hours after 5-FU addition. The average cell death percentage of the Δ*BBC3* clones is 15.61 ± 5.78.

3.8 References

Andreu-Fernandez, V., Garcia-Murria, M., Bano-Polo, M., Martin, J., Monticelli, L., Orzaez, M., Mingarro, I. (2016). The C-terminal Domains of Apoptotic BH3-only Proteins Mediate Their Insertion into Distinct Biological Membranes. *The Journal of Biological Chemistry, 291(48),* 25207-25216. doi: 10.1074/jbc.M116.733634

Bothmer, A., Phadke, T., Barrera, L. A., Margulies, C. M., Lee, C. S., Buquicchio, F., Moss, S., Abdulkerim, H. S., Selleck, W., Jayaram, H., Myer, V. E., & Cotta-Ramusino, C. (2017). Characterization of the interplay between DNA repair and CRISPR/Cas9-induced DNA lesions at an endogenous locus. *Nature communications*, *8*, 13905. https://doi.org/10.1038/ncomms13905

Fagagna, F. (2008). Living on a break: cellular senescence as a DNA-damage response. *Nature Reviews Cancer, 8(7),* 512-522. doi: 10.1038/nature08467.

Fernandes-Alnemri, T., Litwack, G., Alnemri, E. (1994). CPP32, a novel human apoptotic protein with homology to Caenorhabditis elegans cell death protein Ced-3 and mammalian interleukin-1 beta-converting enzyme. *Journal of Biological Chemistry, 269(49),* 30761-30764. PMID: 7983002

Jackson, S., Bartek, J. (2009). The DNA-damage response in human biology and disease. *Nature, 461(7267),* 1071-1080. doi: 10.1038/nature0867

Kuo, L., Yang, Li-Xi. (2008). Gamma-H2AX – a novel biomarker for DNA double-strand breaks. *In Vivo, 22(3),* 305-309. PMID: 18610740.

Nicholson, D., Ali, A., Thornberry, N., Vaillancourt, J., Ding, C., Gallant, M., Gareau, Y., Griffin, P., Labelle, M., Lazebnik, Y., Munday, N., Raju, S., Smulson, M., Yamin, T., Yu, V., Miller, D. (1995). Identification and inhibition of the ICE/CED-3 protease necessary for mammalian apoptosis. *Nature, 376,* 37-43. doi: 10.1038/376037a0

Ran, F. A., Hsu, P. D., Wright, J., Agarwala, V., Scott, D. A., & Zhang, F. (2013). Genome engineering using the CRISPR-Cas9 system. *Nature protocols*, *8*(11), 2281–2308. https://doi.org/10.1038/nprot.2013.143

Stewart-Ornstein, J., Lahav, G. (2016). Dynamics of CDKN1A in Single Cells Defined by an Endogenous Fluorescent Tagging Toolkit. *Cell Reports, 14,* 1800-1811. doi: 10.1016/j.celrep.2016.01.045

Wigmore, P., Mustafa, S., El-Beltagy, M., Lyons, L., Umka, J., Bennett, G. (2010). Effects of 5-FU. *Advances in Experimental Medicine and Biology, 678,* 157-164. doi: 10.1007/978-1-4419-6306-2_20

Yee, K., Vousden, K. (2008). Contribution of membrane localization to the apoptotic activity of PUMA. *Apoptosis, 13,* 87-95. doi: 10.1007/s10495-007-0140-2

Yu, J., Zhang, L., Hwang, P., Kinzler, K., Vogelstein, B. (2001). PUMA Induces the Rapid Apoptosis of Colorectal Cancer Cells. *Molecular Cell, 7,* 673-682. doi: 10.1016/s1097-2765(01)00213-1

Yuan, J., Adamski, R., Chen, J. (2010). Focus on histone variant H2AX: to be or not to be. *FEBS Letters, 584(17),* 3717-3724. doi: 10.1016/j.febslet.2010.05.021

CHAPTER 4 CAP-INDEPENDENT TRANSLATION OF PUMA-α FROM AN INTERNAL AUG

4.1 Rationale

Previous study from our lab has shown that cisplatin induces *PUMA-α* mRNA without increasing PUMA-α protein in renal epithelial cells where nuclear localization of Abl is blocked by germline mutations of the nuclear localization signals in the mouse *Abl1* gene. (Sridevi et al., 2013). This result suggests that *PUMA-α* translation may be regulated by a nuclear Abl-dependent mechanism in DNA damage response. Inspection of *PUMA-α* sequence reveals an upstream open reading frame (uORF) of 41 amino acids in Exon-1a of *BBC3* (Figure 4.1). If this uORF in the PUMA-α mRNA were to be translated, then, the translation of PUMA-α ORF would have to initiate from an internal AUG.

To determine if the uORF in Exon-1a is translated, I applied the eFLUT technology (Steward-Ornstein & Lahav, 2016) using CRISPR/Cas9, to insert an AUG-less ORF of Venus_p2a_Neo (VpN) into the uORF at the C-terminus and upstream of the uORF termination codon. Following Cas9-cutting and VpN insertion through homology directed repair (HDR), the Exon-1a-edited *BBC3* would be expected to encode a longer uORF of 577 amino acids. If the AUG of the uORF is functional as a translation initiation codon, then, in-frame ligation of the uORF with the VpN ORF would lead to the expression of an uORF-Venus fusion protein and a Neomycin-Resistance factor (Neo) due to the self-cleavage activity of the p2a peptide (Steward-Ornstein & Lahav, 2016). As a result, such Exon-1a edited cells would become resistant to G418. By selection of edited clones for G418-resistance, followed by verification of Neo insertion into the *BBC3* Exon-1a, and the expression of Neo and Venus, it is possible to show that the AUG of the uORF in *BBC3* Exon-1a is translated.

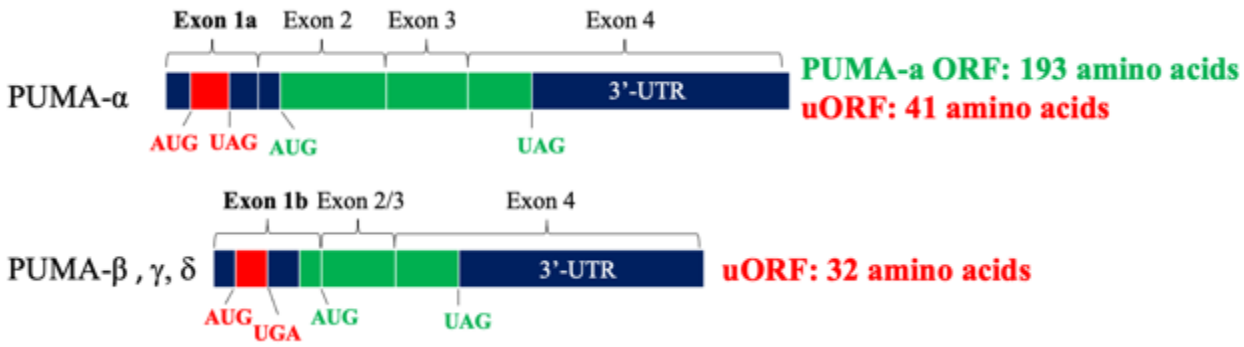

Figure 4.1 Upstream Open Reading Frames (uORFs) in PUMA mRNAs.

4.2 Selection of sgRNA for the Insertion of the Venus_p2a_Neo ORF into *BBC3* Exon-1a

A single sgRNA was selected to edit Exon-1a at the C-terminus of the uORF with its on-target efficacy score and off-target rankings determined by the Broad Institute sgRNA portal (https://portals.broadins titute.org/gpp/public/analysis-tools/sgrna-design). The sgRNA is named by the oligonucleotides used for cloning, e.g., sgRNA 13/14 denotes the sgRNA coding fragment annealed from oligonucleotides 13 and 14 and has an on-target efficacy score of 0.6067 and an off-target rank of 2 (Figure 4.2). When expressed as a CRISPR with the Cas9-binding scaffold RNA, sgRNA 13/14 guides Cas9 nuclease to make a cut 7 bp upstream of the uORF stop codon (Figure 4.2).

4.3 Construction of sgRNA-Expressing Plasmids

Oligo-13 and 14 were annealed together to form annealed sgRNA oligos 13/14. This oligo was then ligated into pSpCas9(BB)-2A-Puro following digestion of the plasmid with BbsI which removed the restriction sites and allowed for the direct insertion of the annealed sgRNA oligo between the U6 promoter and the CRISPR scaffold sequence to form an sgRNA-expressing plasmid. This plasmid was then transformed into Subcloning Efficiency DH5α

competent cells (ThermoFisher Scientific) and transformed cells were grown on LB-Ampicillin plates. Three randomly picked bacterial colonies were selected for plasmid extraction and were verified by restriction enzyme digestion with BbsI. Successful insertion of the sgRNA oligo into the pSpCas9(BB)-2A-Puro vector destroys the BbsI recognition sites. Therefore pSpCas9(BB)-2A-Puro vector with the annealed sgRNA oligo inset cannot be digested by BbsI into linear DNA. The restriction digestion verified plasmids were further verified by Sanger sequencing (Retrogen) to confirm that the sgRNA 13/14 oligo insert has the correct nucleotide sequence.

Larger quantities of DNA were generated in preparation for transfection using midiprep. BbsI digestion and Sanger sequencing were again used to verify successful insertion of the sgRNA oligos and correct nucleotide sequences. BglII digestion was also performed to verify the size of linearized sgRNA 13/14 expressing plasmid constructs. The sgRNA 13/14 expressing plasmid was able to be linearized by BglII with the expected band size of ~9000 bp on gel electrophoresis.

4.4 PCR Amplification of the Venus_p2a_Neo from a Donor Plasmid

To obtain sufficient amounts of the Venus_p2a_Neo (VpN) ORF for transfection with the sgRNA 13/14-Cas9-plasmid, PCR primers were used to amplify the VpN sequence from a 4263 bp donor plasmid provided by the Stewart-Ornstein & Lahav lab (Table 2.1). The forward and the reverse primer each contains a 60 bp homology arm that is identical to the Exon-1a sequence. The forward primer aligns with the 60 bp sequence that is immediately upstream of the sgRNA-13/14-directed Cas9-cut site. The reverse primer aligns with the 60 bp sequence that starts 6 bp downstream of that cut site (Figure 4.2). The reverse primer was designed this way to allow for an in-frame termination codon with the Neo ORF. The forward primer also contains 30sequences

located immediately upstream of the VpN ORF in the donor plasmid, whereas the reverse primer contains 30 sequences located immediately downstream of the VpN ORF in the donor plasmid (Figure 4.2). The PCR product of 1772 bp is gel-purified for transfection into HCT116 cells with the sgRNA-13/14-Cas9 plasmid.

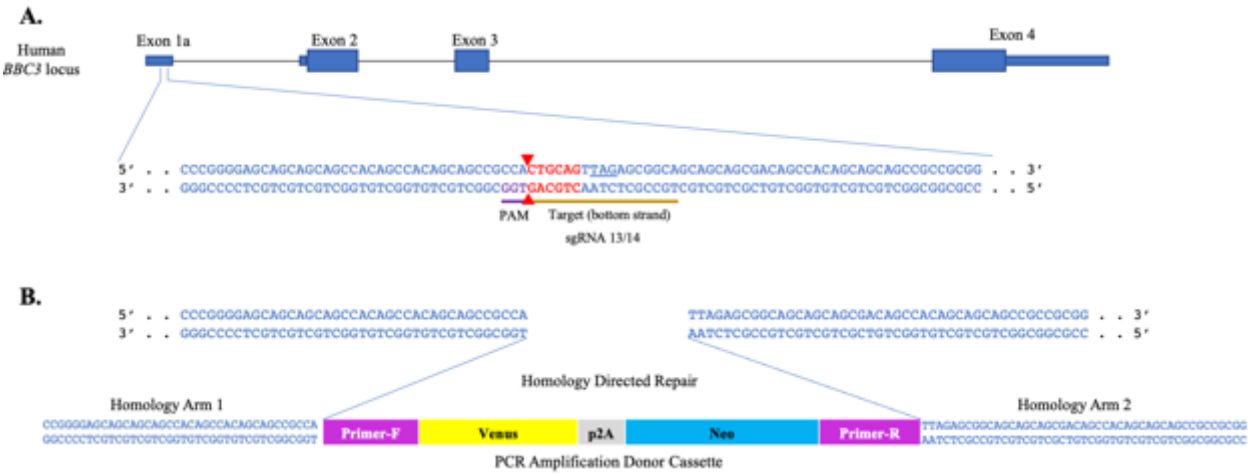

Figure 4.2 Editing Exon-1a of *BBC3* by Insertion of Venus-p2A-Neo Cassette. (A) Schematic of PUMA-α exons with larger boxes depicting PUMA-α open reading frame (ORF) and smaller boxes depicting un-translated sequences. Note that Exon-1a contains an upstream ORF (uORF) of 126 nucleotides. The translation termination codon TAG of that uORF is underlined in the depicted sequences below the diagram. The gRNA 13/14 was selected to introduce a cut 7 base pairs upstream of that termination codon. The red triangles denote the CAS9 cut site. Following CAS9-cutting and recombination with the PCR fragment containing homology arms and the Venus-p2A-Neo cassette (see B), six base pairs (colored in red) will be lost. (B) The ORF of Venus-p2A-Neo is PCR amplified with primers containing 60 bp homology arms to generate a 1772 bp DNA fragment. The left homology arm is immediately upstream of the CAS9-cut site in Exon-1a. The right homology arm is six-base pair downstream of the CAS9-cut site as depicted in (A). Primer-F and Primer-R are present in the Venus-p2A-Neo donor plasmid and anchor the homology arms to amplify the desired PCR fragment for insertion into *BBC3* Exon-1a through homologous recombination.

4.5 Selecting and Characterizing *BBC3-Exon-1a*-Edited Clones

HCT116 cells were transfected with both the sgRNA-13/14/Cas9 plasmid and the Venus_p2a_Neo ORF by lipofectamine, with a control transfection with the sgRNA-13/14/Cas9 plasmid alone and a mock transfection with lipofectamine alone. At 24 hours post transfection,

cells were split into puromycin containing media for 48 hours to select for plasmid-transfected cells. Only the cells transfected with the sgRNA-13/14/Cas9 plasmid were expected to survive the puromycin treatment because the pSpCas9(BB)-2A-Puro plasmid expressed a puromycin resistance factor (Puro). After 48 hours of puromycin treatment, when all mock-transfected cells died, surviving cells were treated with the antibiotic Geneticin (G418) for 6 days to select for cells that express the Neomycin resistance gene (Neo). Acquisition of G418-resistance in transfected cells can only occur when the VpN ORF is fused in-frame with a translated ORF in the genome. Following G418 selection, surviving cells were seeded at low density in 96-well plates to obtain single clones. Once colonies that formed from single cells became 30% confluent, they were split for genomic PCR screening and propagation.

To ascertain the VpN ORF is inserted into *BBC3* Exon-1a, genomic DNA was extracted from the G418-resistant clones and subjected to PCR reactions using a forward primer from Neo and a reverse primer from Intron 1-2 of *BBC3* (Figure 4.3A, Table 4.1). If the VpN ORF is properly inserted by HDR, the expected length of the genomic PCR products from the *BBC3-Exon-1a*-edited clones is 255 bp. Of the 22 clones screened, only 5 clones showed detectable PCR products with sizes around 255 bp as summarized in Table 4.2. These clones were referred to as clone E1a-C3, E1a-C8, E1a-C9, E1a-C17, and E1a-C19.

The PCR fragments from the *BBC3-Exon-1a*-edited clones were cloned into the TOPO vector. Light blue colonies on LB Ampicillin and X-Gal plates were selected and their plasmids extracted and sequenced (Figure 4.4). Alignment of the PCR fragment sequence to the *BBC3* Exon-1a and the VpN sequences, shown in Figure 4.4B, showed imperfect HDR during editing. In E1a-C3, the 3'-end of Neo and Primer R sequences (Figure 4.2) and Exon-1a were lost and replaced with sequences of unknown origin during insertion into *BBC3*. IN E1a-C8, 39 bp of

foreign sequences were added into the 3'-region of Exon-1a, consistent with the larger than expected PCR size observed in Figure 4.3. In E1a-C9, the insertion appeared to have resulted from a perfect HDR. In E1a-C17, the insertion led to a 4 bp deletion in the 3'-region of Primer R sequences.

Attempts to amplify a genomic fragment from the 5'-end of Exon-1a to the Venus coding sequence have failed due to the fact that Exon-1a and its upstream genomic sequences have a G/C content of 80%. I tried to overcome this G/C block by conducting PCR reactions with different polymerases and different DMSO concentrations without success. Therefore, the 5'-region of the Exon-1a-edited *BBC3* alleles remain to be characterized.

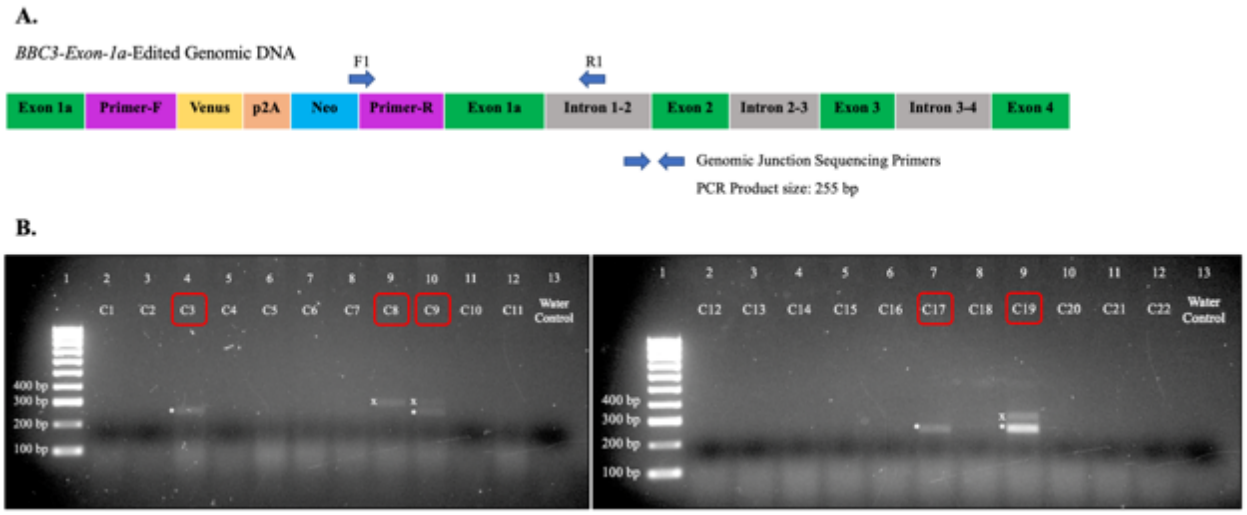

Figure 4.3 Identifying *BBC3-Exon-1a*-Edited Clones by Genomic PCR. (A) Positions of junction primers for amplifying desired *BBC3-Exon-1a*-edited clones. The forward primer (F1) contains 14 bp of the Neomycin sequence and 6 bp of the Primer-R sequence surrounding the termination codon of the uORF. The reverse primer (R1) contains 20 bp of sequence in Intron 1-2. The expected PCR product size is 255 bp. (B) Junction primer-derived genomic PCR fragments from single cell clones following co-transfection with the sgRNA-13/14 targeting plasmid and the homology-arm-flanked Venus-p2A-Neo DNA fragment. Bands marked with * are the same bp length as the expected PCR product. Bands marked with X are longer in bp length compared to the expected PCR product. Five potential clones (boxed in red) were selected for expansion and sequencing.

Table 4.1 Sequence of Junction Primers Used to Screen for *BBC3-Exon-1a*-Edited Clones.

	Primer Sequence
Forward	ATCGCCTTCTTGACGAGTTC
Reverse	TGCACTCCTGTCACCTCCTC

Table 4.2 Summary of Genomic PCR Analysis of *BBC3-Exon-1a*-Edited Clones.

Clone	E1a-3	E1a-8	E1a-9	E1a-17	E1a-19
# PCR products	1	1	2	1	2
Size of PCR products	255 bp	280 bp	255, 280 bp	255 bp	255, 310 bp

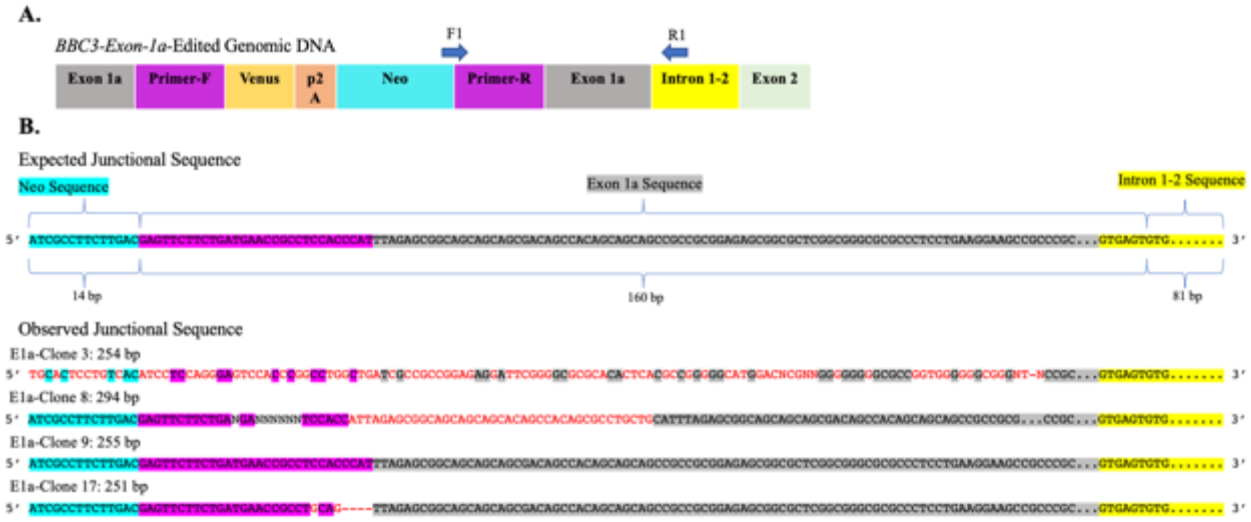

Figure 4.4 Genomic Junction Sequences in *BBC3-Exon-1a*-Edited Clones. (A) PCR primers used to amplify the genomic DNA containing Neo and *BBC3* Exon 1 sequences. The forward primer (F1) contains 14 bp of the Neo sequence and 6 bp Primer-R sequence. The reverse primer (R1) contains 20 bp of Intron 1-2 sequence. In the expected PCR products, 14 bp aligns with the Neo sequence (highlighted in blue), 30 bp aligns with Primer-R sequence (pink) 130 bp aligns with the Exon-1a sequence (highlighted in gray), and 81 bp aligns with the Intron 1-2 sequence (highlighted in yellow). (B) Junctional sequence variation in four *BBC3-Exon1a*-edited clones analyzed. Nucleotides that different from the expected junctional sequence are in red letters. "N" denotes nucleotides that could not be identified by Retrogen Sequencing. E1a-Clone 3 lost one nucleotide (marked as -) and has multiple nucleotides that do not align with the expected junctional sequence as a result of double-cutting and Venus_p2A_Neo cassette insertion. E1a-Clone 8 gained 39 nucleotides. The observed junctional sequence of E1a-Clone 9 is identical to the expected junctional sequence of *BBC3-Exon-1a*-edited genomic DNA. E1a-Clone 17 lost 4 nucleotides and has 2 nucleotides that do not align with the expected junctional sequence.

4.6 Transcription of Venus_p2a_Neo Sequence in *BBC3-Exon-1a*-Edited Clones

To determine if the inserted VpN ORF is transcribed, I extracted total RNA from the *BBC3-Exon-1a*-edited clones, converted the RNA to cDNA and amplified the cDNA with primers from Venus and Neo to detect a predicted 487 bp product (Figure 4.4). The positions of the primers in the VpN ORF is shown in Figure 4.5A. Based on the PCR results shown in Figure 4.5B, the expected PCR product of 487 bp was detected in every *BBC3-Exon-1a*-edited clone (E1a-C3, E1a-C8, E1a-C9, E1a-C17). To control for potential amplification of this 487 bp fragment from the genomic DNA, PCR reactions were conducted with RNA samples not

converted to cDNA by omitting reverse transcriptase (RT) from the cDNA synthesis reactions. As shown in Figure 4.5, a very faint band of 487 bp could be detected in PCR reactions from no-RT controls, showing that the RT-dependent 487 bp PCR product was derived from amplification of cDNAs.

The PCR products were then cloned into the TOPO vector and transformed into chemically competent bacteria. Light blue colonies on LB Ampicillin and X-Gal plates were picked for plasmid extraction and sequencing. The NCBI BLAST tool (https://blast.ncbi.nlm.nih.gov/Blast.cgi) was then used to verify that the sequenced products align with Venus, p2a, and Neo sequences. Based on the PCR and the Sanger sequencing results, the Venus_p2a_Neo ORF was transcribed in each one of the *BBC3-Exon-1a*-edited clones.

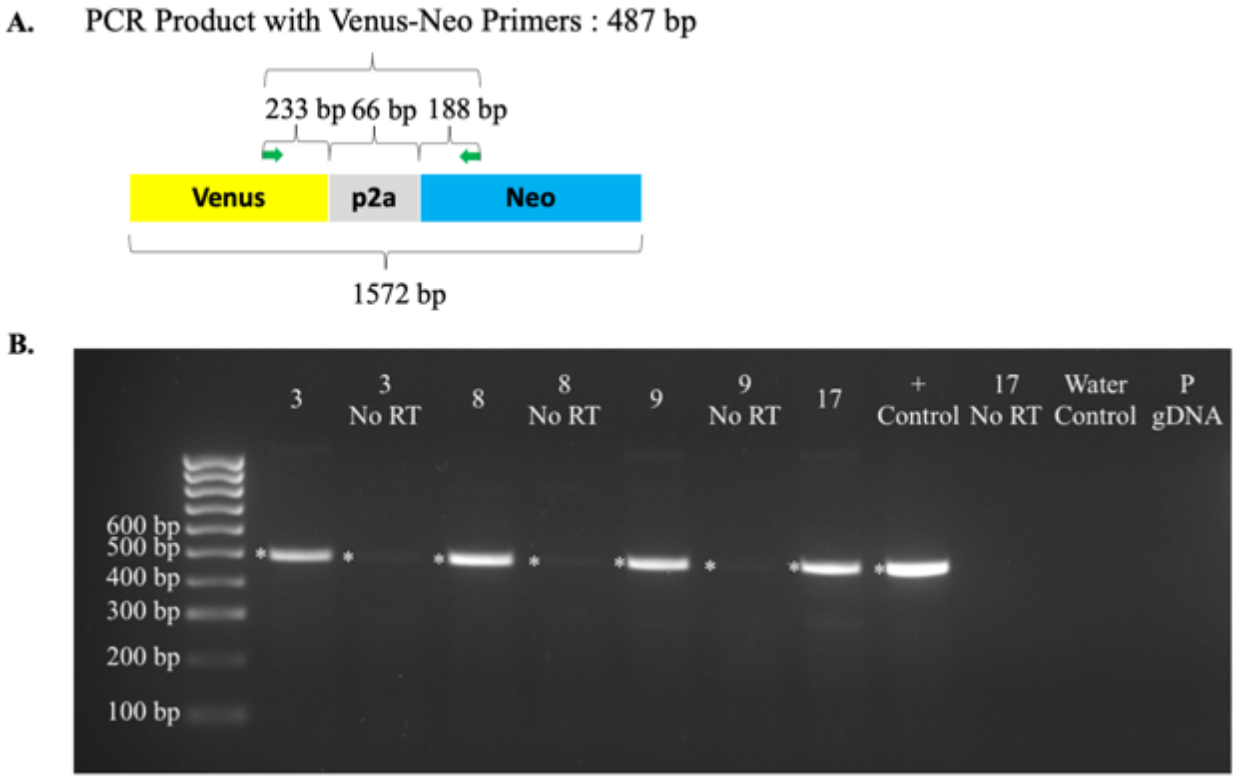

Figure 4.5 Figure 4.5 Detection of Venus_p2a_Neo Open Reading Frame from cDNA of *BBC3-Exon-1a*-Edited Clones. (A) Positions of primers for detection of Venus_p2a_Neo open reading frame. (B) PCR fragments produced from the cDNA of *BBC3-Exon-1a*-edited clones following total RNA extraction. Bands marked with * are the same bp length as the expected Venus_p2a_Neo PCR product. The donor plasmid containing the Venus_p2a_Neo sequence was used as the template in PCR for the positive control. Genomic DNA from parental HCT116 cells was extracted and used as the template in PCR for the negative control.

4.7 DNA Damage-Induced Expression of Neo in *BBC3-Exon-1a*-Edited Clones

Because the VpN ORF is inserted into Exon 1a, whose transcription is stimulated by p53 in response to DNA damage, expression of the Venus and Neo proteins was expected to be induced by DNA damage in the *BBC3-Exon-1a*-edited clones. To test this, I treated cells with 5-FU and then probed whole cell lysates (WCL) with an anti-Neo antibody. *BBC3-Exon-1a*-edited HCT116 clones (E1a-C3, C8, C9, C17), vector transfected control clone (cC1), and parental HCT116 cells were treated with 385 μM 5-FU for 24 hours. Cells were then harvested and whole

cell lysates (WCLs) were probed with anti-Neo and anti-GAPDH (loading control). Probing with anti-Neo resulted in the detection of a 30 kDa band only in the Exon-1a-edited clones and a lower band found in all cells (Figure 4.7), indicating that the 30 kDa band was the product of the Neo gene and the lower band being a non-specific cross-reaction . The expression of Neo was increased following 5-FU treatment, showing that DNA damaging agent can increase Neo levels, lending credence to the notion that Neo was expressed from the E1a-edtied *BBC3* gene. The detection of Neo with the expected molecular weight of 30 kDa from the VpN fusion ORF also indicated that the p2A-self cleaving peptide was able to separate the Neo polypeptide from the Venus poly-peptide as would be expected.

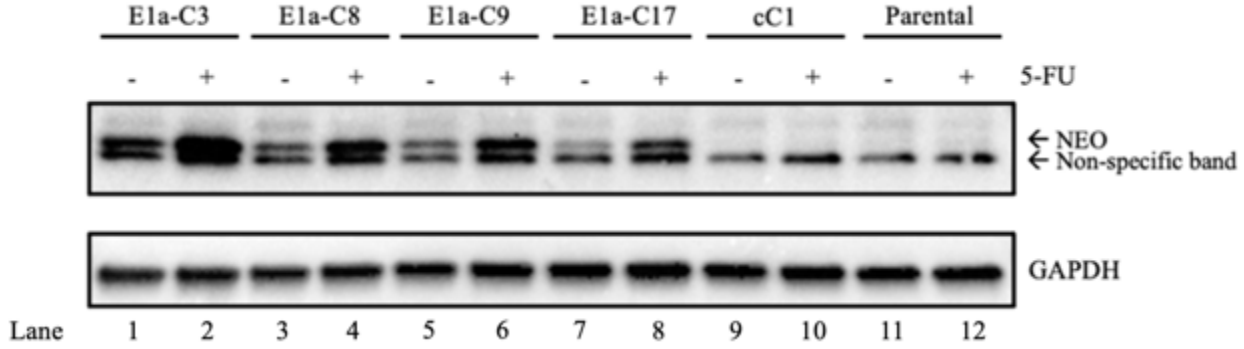

Figure 4.6 Basal and DNA Damage-Induced Expression of Neo in *BBC3-Exon-1a*-Edited Clones. *BBC3-Exon-1a* edited HCT116 clones (E1a-3, 8, 9, 17), control clone (cC1), and parental HCT116 cells (Parental) were treated with vehicle (-) or 385 μM 5-fluorouracil (5-FU) for 24 hours. Cells were then harvested for and whole cell lysates probed with anti-Neo or anti-GAPDH antibodies as indicated. The Neo protein of expected size 30 kDa was detected in the *BBC3*-edited HCT116 clones (E1a-C3, 8, 9, 17) but not in the control clone or the parental HCT116 cells. Expression of the Neo protein was increased following treatment with the DNA damaging agent 5-FU.

4.8 Detection of Venus Fluorescence in *BBC3-Exon-1a*-Edited Clones

Having confirmed the transcription of the Venus_p2a_Neo (VpN) ORF and detection of Neo protein expression, I examined the expression of Venus by live cell imaging with a

fluorescence microscope. I seeded cells from the Exon-1a-edited E1a-C3, E1a-C8 and control clones cC1 and cC2 in duplicates into a chamber slide and treated half of the chambers with vehicle (DMSO), the other half of the chambers with 5-FU, and performed live-cell imaging 24 hours after drug addition. As shown in Figure 4.7A, yellow fluorescence was detected throughout the cytoplasm and nucleus of cells from the edited E1a-C3 and E1a-C8 clones, whereas punctate fluorescence signals were found in cells from the control cC1 and cC2 clones. The fluorescence intensities in E1a-C3 and E1a-C8 cells were visibly higher in 5-FU treated samples, whereas the punctate signals in cC1 and cC2 clones were not detectably altered by 5-FU treatment. The fluorescence signals in these live cell images were analyzed by ImageJ where above-background fluorescence was defined as having a pixel intensity ≥ 265 with a maximum of 65,535 (Figure 4.7B). In the images of E1a-C3 cells, 13.8% of pixels showed above-background intensities in DMSO-treated sample, whereas 22.3% of pixels were above background in 5-FU treated sample, indicating a 2-fold increase in Venus fluorescence in response to DNA damage. In the images of E1a-C9 cells, 0.1% of pixels were above background in DMSO-treated sample, whereas 1.9% of pixels were above background after 5-FU treatment, indicating a 20-fold increase in Venus fluorescence in this Exon-1a-edited clone. In the images of the two control clones, between 0.1 to 1% of the pixels showed above-background intensities, which were not increased in 5-FU treated samples (Figure 4.7B). These results further suggested that the inserted VpN ORF was translated to generate the fluorescent Venus protein in *BBC3* Exon-1a-edited clones.

In a second live-cell imaging experiment that was conducted months later, after serial freezing and thawing of the E1a-edited clones, yellow fluorescence was again detected in E1a-C3, C8, C9, C17 and in the pool of G418-resistant cells prior to cloning (Figure 4.8). However,

when compared to the signal from HCT116 cells transiently transfected with a Venus-H2B-expression plasmid, the signal from the inserted VpN ORF was considerably lower (Figure 4.8). The weak but reproducible detection of yellow fluorescence from the Exon-1a-edited clones confirmed that the VpN ORF is translated.

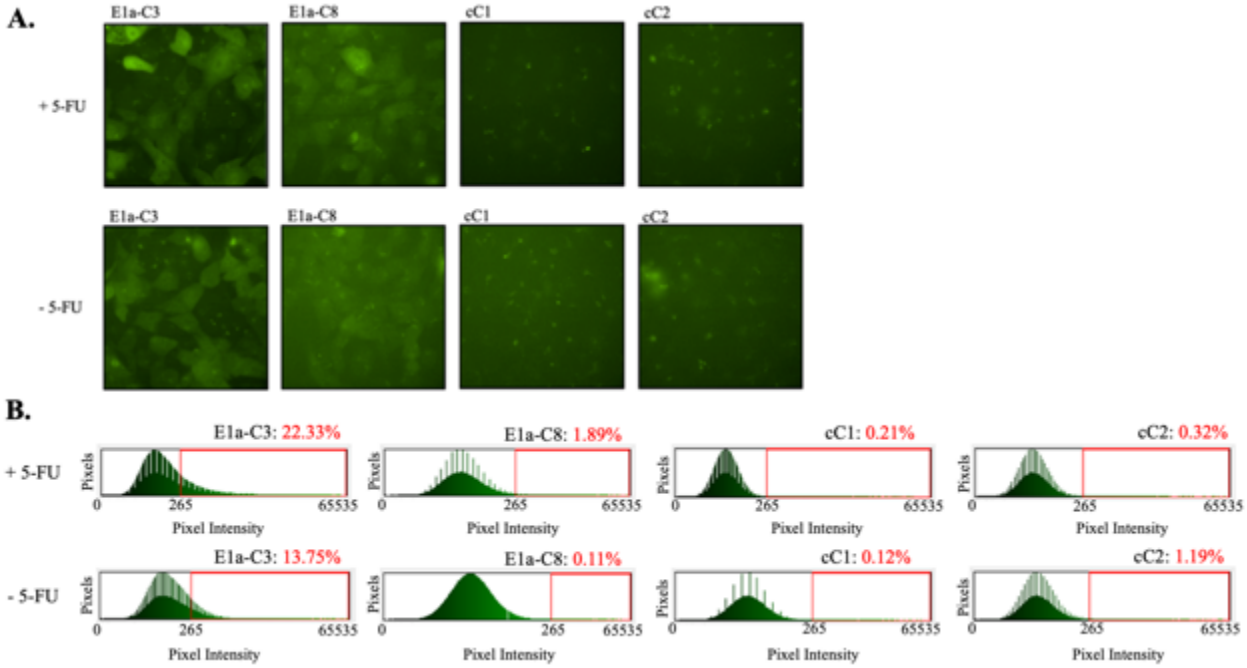

Figure 4.7 Detection of Venus Expression by Fluorescence Microscopy. (A) Two *BBC3-Exon-1a*-edited clones, i.e., E1a-C3 and 8 as well as two vector transfected control clones (cC-1, 2) were treated with or without 385 µM 5-FU in one chamber slide. Live cells images were captured 24 hours after drug treatment using filters for YFP fluorescence. (B) Fluorescence image quantification using ImageJ. The x-axis shows pixel intensity, and the y-axis shows the number of pixels at each intensity. Background fluorescence is set at a pixel intensity of < 265. Positive fluorescence detection is defined as having a pixel intensity ≥ 265 and the maximum pixel intensity is 65535. The red box denotes pixels that have pixel intensity between 265 and 65535. The percentage of positive fluorescence pixels in each image is shown besides each clone name in red.

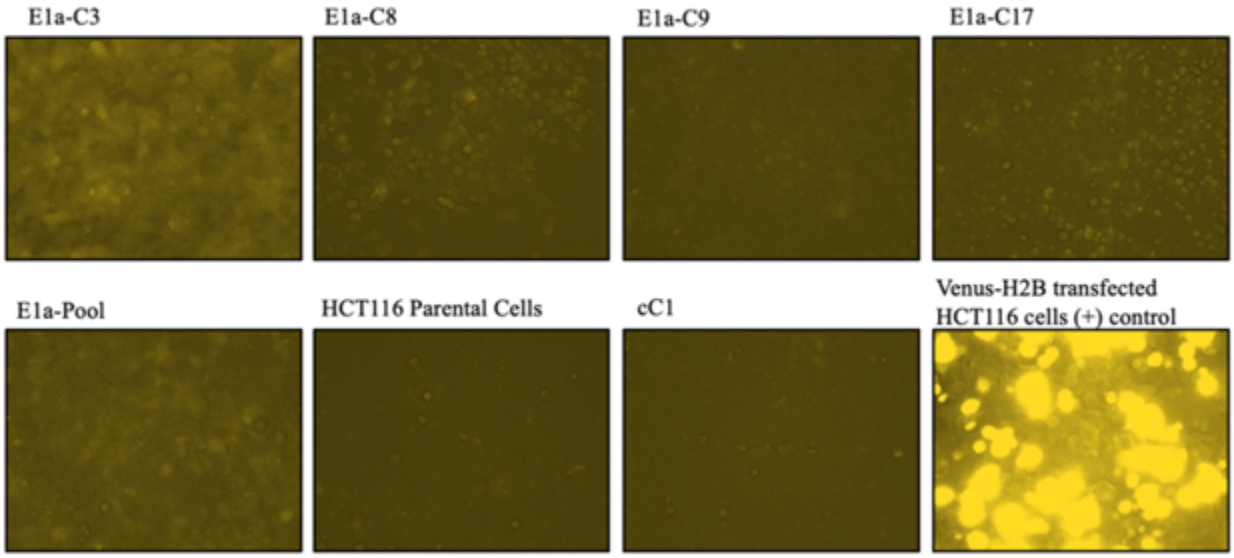

Figure 4.8 Venus Fluorescence Signals of *BBC3-Exon-1a*-Edited Clones Following Serial Freezing and Thawing. The *BBC3-Exon-1a*-edited clones 3, 8, 9, 17, the *BBC3-Exon-1a*-edited pool of cells without cloning, the Parental HCT116 cells, the control clone 1 and Parental HCT116 cells transiently transfected with Venus-H2B expression plasmid were seeded in chamber slide and live cell images were captured 24 hours after seeding using the ECHO Revolve Microscope with an YFP-cube.

4.9 DNA Damaged-Induced Expression of PUMA-α in *BBC3-Exon-1a*-Edited Clones

After determining that the Venus_p2a_Neo is both transcribed and translated I wanted to determine if the insertion of this large Venus_p2a_Neo cassette (1772 bp) into Exon 1a affected the expression of PUMA-α protein. To do so, I treated the *BBC3-Exon-1a*-edited clones E1a-C3, E1a-C8, E1a-C9, E1a-C17, a control clone (cC1), and the parental HCT116 cells with 385 μM 5-FU for 24 hours and then probed whole cell lysates with anti-PUMA-α and anti-GAPDH (loading control). As shown in Figure 4.9, PUMA-α was still expressed in the *BBC3-Exon-1a*-edited clones and it levels were still induced by 5-FU. It is possible that a wild-type allele of the *BBC3* gene remains in each of the Exon-1a-edited clones, that is, the editing only occurred on one of the two *BBC3* alleles, and the PUMA-α protein was expressed from the un-edited *BBC3*. Alternatively, if the editing affected both alleles of *BBC3*, then, PUMA-α protein would have to

be expressed from the Exon-1a edited *BBC3*, either from a bi-cistronic mRNA containing a fused uORF-VpN-ORF on the 5'-end and the PUMA-α-ORF on the 3'-end. Without direct evidence for the existence of such a bi-cistronic mRNA, it is not possible to conclude that translation of the fused uORF-VpN-ORF cannot interfere with translation of the downstream PUMA-α ORF. Nevertheless, results shown in Figures 4.5 to 4.8 strongly suggest that the VpN-ORF is transcribed and translated from Exon-1a of the *BBC3* gene.

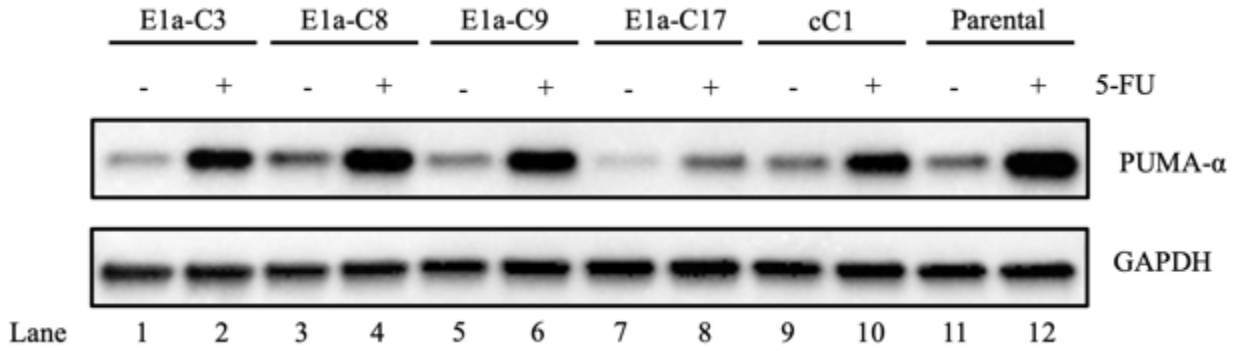

Figure 4.9 Basal and DNA Damage-Induced Expression of PUMA-α in *BBC3-Exon-1a*-Edited Clones. *BBC3-Exon-1a*-edited HCT116 clones (E1a-3, 8, 9, 17), control clone (cC1), and parental HCT116 cells (Parental) were treated with vehicle (-) or 385 μM 5-fluorouracil (5-FU) for 24 hours. Cells were then harvested for and whole cell lysates probed with anti-PUMA-α or anti-GAPDH antibodies as indicated. The PUMA-α protein of expected size 24 kDa was detected in the *BBC3*-edited HCT116 clones (E1a-C3, 8, 9, 17). Expression of the PUMA-α protein was increased following treatment with the DNA damaging agent 5-FU.

4.10 CAP-Independent Translation of PUMA-α ORF

In eukaryotes, mRNA translation typically initiates from the 5'-most AUG or GUG codon because loading of the 43S pre-initiation ribosome complex requires the eIF4F complex which is positioned at the 5'-end of mRNA through binding of eIF4E to the 5'-CAP structure (Sriram et al., 2018). Recent studies have found that translation from an internal AUG or GUG can also occur in eukaryotic cells through multiple different mechanisms that can be loosely

divided into two categories as (a) Leaky Scanning or (b) Re-initiation (Citations). In Leaky Scanning, ribosomes are loaded onto the mRNA via the 5'-CAP binding complex (CAP-dependent) but can skip the most proximal AUG to begin translation at an internal AUG (Sriram et al., 2018). In Re-initiation, ribosomes are loaded onto the internal AUG by "re-initiation factors" that do not interact with the 5'-CAP (CAP-independent). In order to distinguish between the two mechanisms, I experimented with a compound, 4EGI-1. This compound disrupts the interaction of eIF4E and eIF4G, both are components of the eIF4F complex that is required for CAP-dependent translation (Moerke et al., 2007). Although eIF4G can interact with other factors to stimulate translation initiation, disruption of its interaction with eIF4E, which directly binds to the CAP-structure, interferes with CAP-dependent translation initiation (Figure 4.10) (Sekiyama et al., 2015). If the internal PUMA-α AUG is recognized through Leaky Scanning, 4EGI-1 would be expected to inhibit the expression of PUMA-α protein. On the other hand, if the internal PUMA-α AUG is recognized through Re-initiation, then 4EGI-1 would not be able to inhibit expression of PUMA-α protein.

Based on previously published studies, the inhibitory effect of 4EGI-1 on protein levels was not observed until 6-8 hours after drug addition (Moerke et al., 2007; Sekiyama et al., 2015). Furthermore, pro-longed treatment with 4EGI-1 appeared to stress the cells and could induce p53 (Harris et al., 2018). Since the low basal PUMA-α protein levels can be difficult to detect, it is necessary to determine how 4EGI-1 may affect 5-FU-induced PUMA-α protein expression. Therefore, I developed a protocol where cells were pre-treated with 4EGI-1 (or DMSO) for 4 hours, followed by treatment with 5-FU (or DMSO) for 12 hours (Figure 4.11A). I then collected whole cell lysates (WCL) and total RNA from the DMSO/DMSO, 4EGI-1/DMSO, DMSO/5-FU, and 4EGI-1/5-FU treated cells for analysis of proteins by Western blotting (Figure

4.11B and RNAs by real-time quantitative RT-PCR (Figure 4.12). Treatment with 50 μM of 4EGI-1 did not affect the levels of GAPDH, however, treatment with 100 μM of 4EGI-1 reduced the levels of GAPDH by about two-fold. Since GAPDH translation is most likely to be CAP-dependent, this 4EGI-1 dose-dependent reduction in GAPDH protein levels indicated a partial inhibition of CAP-dependent translation by this compound in HCT116 cells. I included anti-MYC in the blotting experiment because a previous study showed that 50-100 μM 4EGI-1 reduced MYC protein levels in Jurkat T-cells (Moerke et al., 2007). However, in HCT116 cells, the inhibitory effect of 4EGI-1 on MYC expression was not as robust as that reported in Jurkat cells (Figure 4.11B).

Treatment with 4EGI-1 did not reduce the basal, un-induced, levels of p53, p21CIP1 and PUMA-α, whereas treatment with 5-FU significantly increased the levels of p53, p21CIP1 and PUMA-α in HCT116 cells (Figure 4.11B). When cells were treated with 4EGI-1 and 5-FU, p53 and p21CIP1 levels were reduced, whereas PUMA-α levels were not reduced (Figure 4.11B). To quantify the effects of 4EGI-1 on 5-FU-induced PUMA-α, p53, and p21CIP1 protein levels, I measured the band intensities using ImageJ and normalized them to that of GAPDH . Since 4EGI-1 at 100 μM reduced GAPDH by two-fold (Table 4.3), the GAPDH band intensities could not be used for normalization in the 100 μM 4EGI-1 experiment. Using normalized band intensities (NBI) from the 50 μM 4EGI-1 experiment and setting the NBI of each protein in DMSO/DMSO-treated sample to 1, the protein fold change was calculated for the 4EGI-1/DMSO and the DMSO/5-FU samples (Table 4.3), I then calculated the "expected" fold change in the 4EGI-1/5-FU samples from those two samples and compared the "expected" to the "observed" fold change measured by immunoblotting (Table 4.3). From this analysis, I found that the expected and the observed PUMA-α protein fold change to be similar, indicating that

4EGI-1 did not affect the 5-FU-induced increases in PUMA-α (Table 4.3) However, the observed fold change of p53 and p21CIP1 was significantly lower than that of the observed fold change, indicating that 4EGI-1 significantly reduced the 5-FU-inducd increases in p53 and p21CIP1 (Table 4.3). Together, the immunoblotting results showed that 4EGI-1 affected the expression of GAPDH, p53 and p21CIP1 but not PUMA-α proteins in HCT116 cells and suggested that PUMA-α translation was likely to occur in a CAP-independent manner.

To ascertain that 4EGI-1 did not affect the levels of GAPDH, p53, p21CIP1, and PUMA-α RNA, I measured RNA levels by real-time quantitative RT-PCR. The raw CT values obtained from real-time RT-PCR with exon-spanning primers for the p53, p21CIP1 and PUMA-α RNA were subtracted by the CT values of GAPDH, and the ΔCT values of each RNA from each drug-treated sample was subtracted by the ΔCT of DMSO/DMSO-treated sample to obtain a ΔΔCT value. The relative level of each RNA was then calculated as 2^-ΔΔCT where ΔΔCT of 0 gives the value of 1 for each RNA in the DMSO/DMSO treated sample. As shown in Figure 4.12, 5-FU increased the PUMA-α and the p21CIP1 RNA as expected, and treatment with 50 μM 4EGI-1 did not significantly affect either the basal or the induced levels of PUMA-α and p21CIP1 RNA. Drug treatments did not significantly alter the p53 or the MYC RNA in this experiment (Figure 4.12).

I then normalized the protein fold change by the relative levels of RNA in each of the four samples from the 50 μM 4EGI-1 experiment (Table 4.4). The RNA normalized protein fold change again showed that 4EGI-1 reduced the 5-FU-induced p21 and p53 protein levels (indicated by the asterisk in Table 4.4) but not the 5-FU-induced PUMA-α protein levels (Table 4.4), confirming that the inhibitory effect of 4EGI-1 on p53 and p21CIP1 was not at the level of RNA expression. Because 4EGI-1 reduced the expression of p53 and p21CIP1 protein, but not

PUMA-α protein, these results suggest that p53 and p21CIP1 translation are CAP-dependent whereas PUMA-α translation is likely to be CAP-independent.

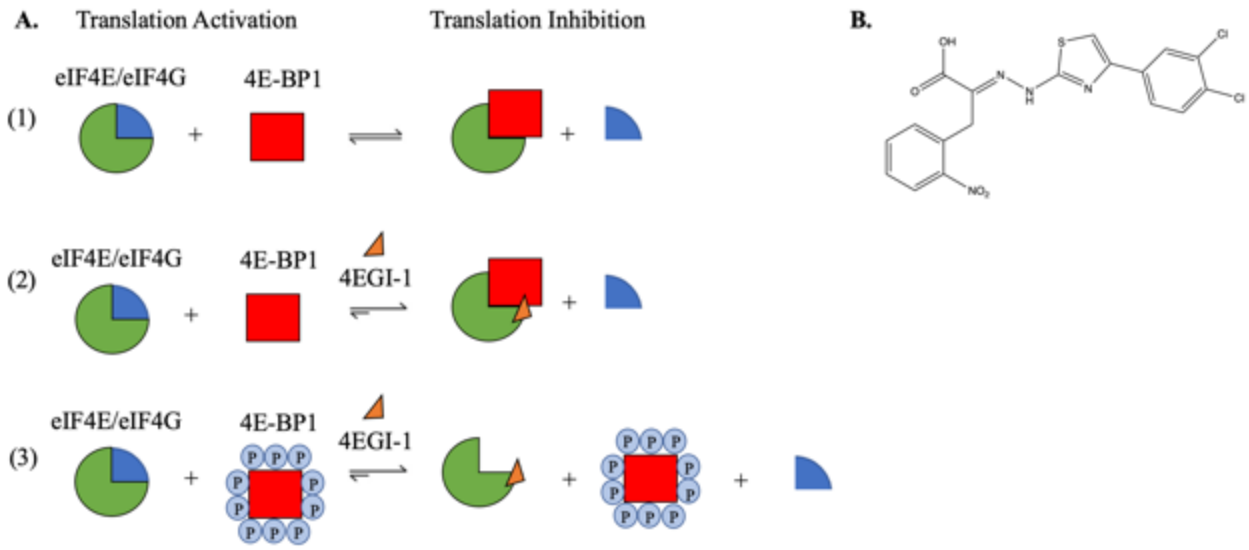

Figure 4.10 Mechanism of 4EGI-1 Inhibition of CAP-Dependent Translation. (A) Visualization of 4EGI-1 function. eIF4E recognizes the 5'-CAP of mRNA and interacts with eIF4G to recruit the small ribosomal subunit to the 5' end of mRNA to initiate translation. 4E-BP1 regulates protein synthesis by competitively binding to eIF4E, reducing eIF4E and eIF4G interaction, thereby inhibiting translation. 4EGI-1 enhances 4E-BP1 binding to eIF4E thereby inhibiting CAP-dependent translation. If 4E-BP1 is serially phosphorylated, preventing it from binding to eIF4E, 4EGI-1 binds to eIF4E and prevents eIF4E and eIF4G interaction. (B) Molecular structure of 4EGI-1.

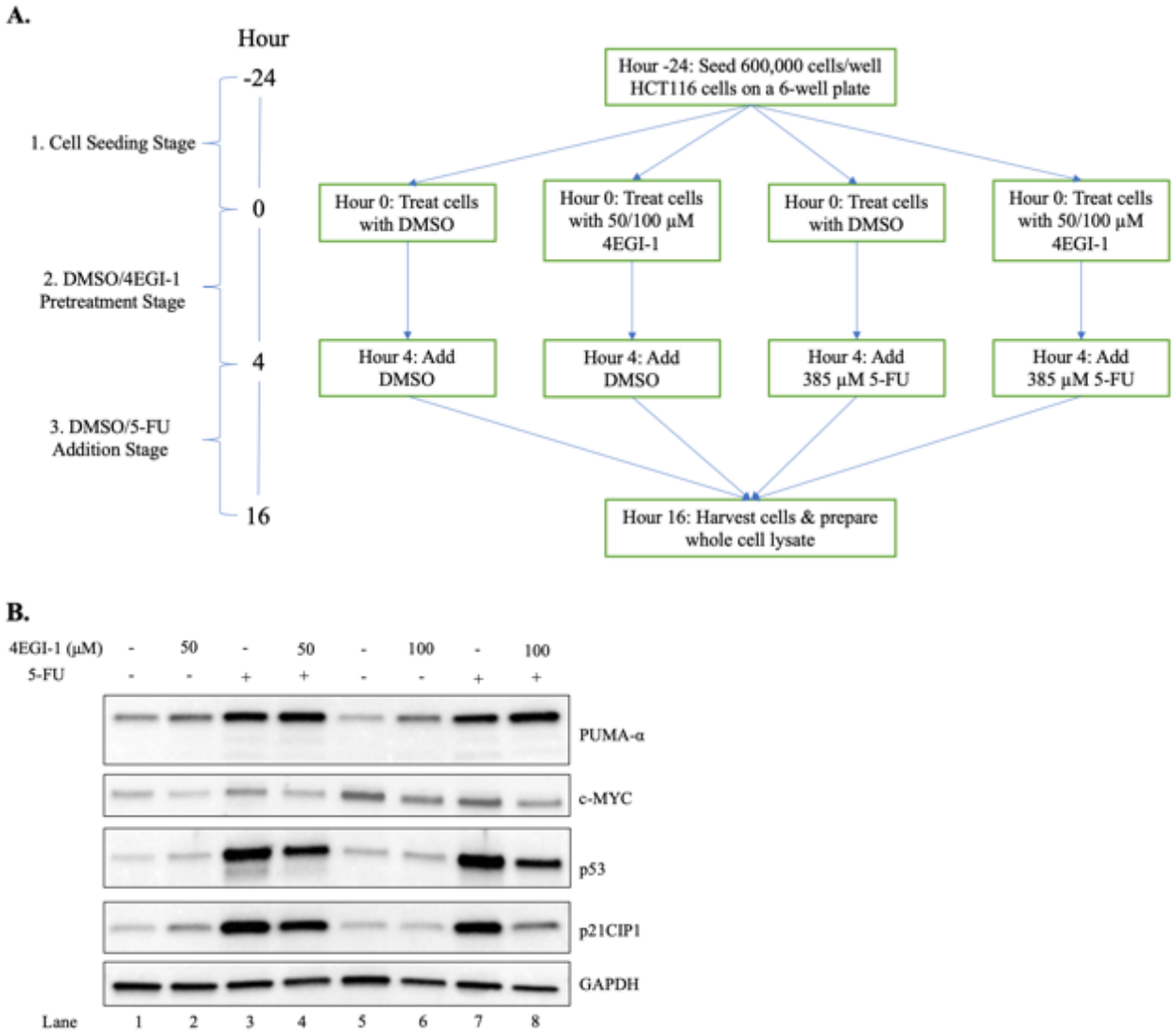

Figure 4.11 Determining the Effects of 4EGI-1 and 5-FU Separately or in Combination on 5-FU Induced Proteins in HCT116 Cells. (A) Experimental design and timeline of DMSO, 4EGI-1, and 5-FU drug addition. HCT116 cells were seeded at 25% confluency 24 hours prior to DMSO/4EGI-1 treatment. Cells were pre-treated with 50/100 µM 4EGI-1 during the pre-treatment stage to maximize the effects of 4EGI-1 before PUMA-α and p21CIP1 mRNAs are induced by 385 µM 5-FU and to minimize the effects of 4EGI-1 itself on p53. The final concentration of the vehicle control (DMSO) is 0.2%. The duration of 4EGI-1 pre-treatment and 5-FU treatment is 4 hours and 12 hours, respectively. (B) Steady-state proteins levels of PUMA-α, c-MYC, p53, p21CIP1. 10 ug of protein was loaded per lane and GAPDH was used as the loading control. 4EGI-1 in combination with 5-FU appears to reduce p53 and p21 steady-state protein levels but not PUMA-α.

Table 4.3 Summary of Protein Fold Change After Treatment with 4EGI-1 and 5-FU Separately or in Combination. Band intensities on Western blots were measured using ImageJ, normalized to that of GAPDH for each blot, and the normalized intensity of each protein in DMSO-treated sample was set to 1. The expected fold change was calculated as the sum of fold change from samples B and C. * Marks fold change observed to be lower than that of expected, indicating an inhibitory effect of 4EGI-1 on 5-FU-induced protein increase.

Treatments	A: 0.2% DMSO	B: 50 µM 4EGI-1	C: 385 µM 5-FU	Expected Fold Change (B-1) +(C-1)+1	D: Observed Fold Change (B, C)
GAPDH	1.00	0.92	0.90	0.88	0.83
PUMA-α	1.00	1.52	2.93	3.45	3.27
c-MYC	1.00	0.50	1.54	1.04	1.00
p21CIP1	1.00	2.07	8.98	10.05	6.86*
p53	1.00	1.70	16.42	17.12	11.11*

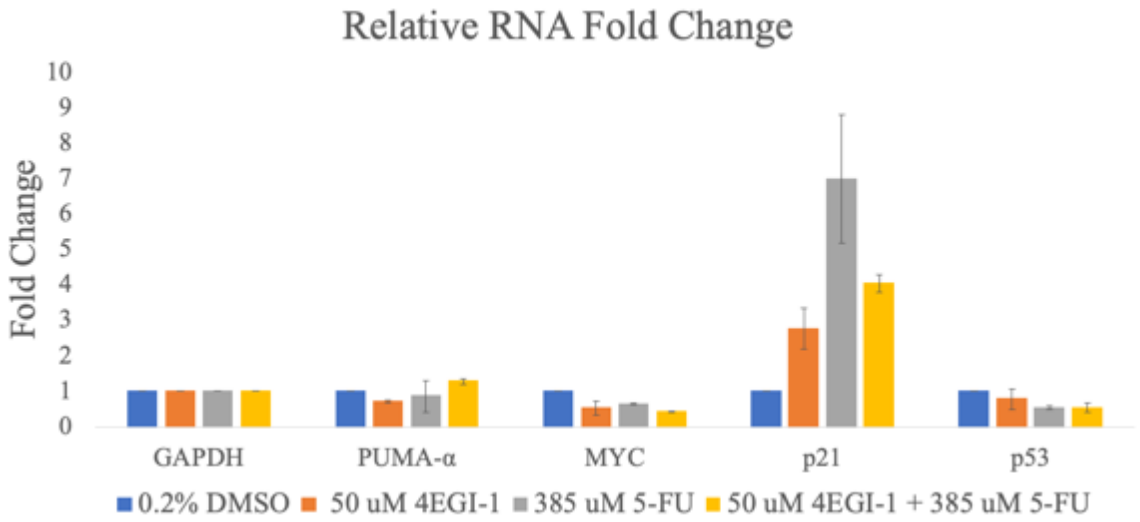

Figure 4.12 Summary of RNA Fold Change After Treatment with 4EGI-1 and 5-FU Separately or in Combination. (A) Summary of RNA fold change with 50 µM 4EGI-1. Total RNA was extracted following drug treatment with 4EGI-1 and 5-FU separately or in combination. 1 µg of RNA per sample was used for RNA to cDNA conversion. SYBR Green was used to measure DNA amplification after each cycle of qRT-PCR. All qRT-PCR primers used were designed to be exon-exon spanning. Three technical repeats were performed for each drug treatment sample. Raw CT values were normalized to that of GAPDH, and each DMSO-treated sample was set to 1.

Table 4.4 Summary of Protein Fold Change Normalized to RNA After Treatment with 4EGI-1 and 5-FU Separately or in Combination. The RNA-normalized protein fold change values were calculated by dividing the protein fold change (Table 2) with their respective relative RNA fold change value (Figure 16). The expected fold change was calculated as the sum of fold change from samples B and C. * Marks fold change observed to be lower than that of expected, indicating an inhibitory effect of 4EGI-1 on 5-FU-induced protein increase.

Treatments	A: 0.2% DMSO	B: 100 µM 4EGI-1	C: 385 µM 5-FU	Expected Fold Change (B-1)+(C-1)+1	D: Observed Fold Change (B, C)
GAPDH	1.00	0.92	1.00	0.90	0.83
PUMA-α	1.00	0.86	2.76	2.62	2.40
c-MYC	1.00	1.03	2.29	2.32	2.14
p21CIP1	1.00	1.24	3.06	3.30	2.08*
p53	1.00	2.39	52.94	54.33	37.68*

4.11 References

Harris, B., Wang, D., Zhang, Y., Ferrari, M., Okon, A., Cleary, M., Wagner, C., Yang, D. (2018). Induction of the p53 Tumor Suppressor in Cancer Cells through Inhibition of Cap-Dependent Translation. *Molecular and Cellular Biology, 38(10),* 1-14. doi: 10.1128/MCB.00367-17

Moerke, N., Aktas, H., Chen, H., Chorev, M., Halperin, J., Wagner, G. (2007). Small-Molecule Inhibition of the Interaction between the translation Initiation Factors eIF4E and eIF4G. *Cell, 128(2),* 257-267. doi: 10.1016/j.cell.2006.11.046

Sekiyama, N., Arthanari, H., Papadopoulos, E., Rodriguez-Mias, R., Wagner, G., Leger-Abraham, M. (2015). Molecular mechanism of the dual activity of 4EGI-1: Dissociating eIF4G from eIF4E but stabilizing the binding of unphosphorylated 4E-BP1. *Proceedings of the National Academy of Sciences of the United States of America, 112(30),* E4036-E4045. doi: 10.1073/pnas.1512118112.

Sridevi, P., Nhiayi, M., Wang, J. (2013). Genetic disruption of Abl nuclear import reduces renal apoptosis in a mouse model of cisplatin-induced nephrotoxicity. *Cell Death Differentiation, 20(7),* 953-962. doi: 10.1038/cdd.2013.42

Stewart-Ornstein, J., Lahav, G. (2016). Dynamics of CDKN1A in Single Cells Defined by an Endogenous Fluorescent Tagging Toolkit. *Cell Reports, 14,* 1800-1811. doi: 10.1016/j.celrep.2016.01.045

Yu, J., Zhang, L., Hwang, P., Kinzler, K., Vogelstein, B. (2001). PUMA Induces the Rapid Apoptosis of Colorectal Cancer Cells. *Molecular Cell, 7,* 673-682. doi: 10.1016/s1097-2765(01)00213-1

CHAPTER 5 DISCUSSION AND FUTURE DIRECTION

5.1 Summary of Results

Applying the CRISPR/CAS9 gene editing technology, I created in the *BBC3* gene of human HCT116 cells (a) C-terminal alterations of PUMA-α ORF, and (b) Exon-1a insertion of a Venus_p2a_Neo ORF. By measuring the cell death response of 5-FU, a DNA damaging agent that activates the p53 -> PUMA-α apoptotic pathway, my thesis research has confirmed the previously reported conclusion that PUMA-α C-terminal amino acids contribute to its pro-apoptotic function. By examining the expression of Venus fluorescence and of the Neo gene product, I showed that the Exon-1a-inserted ORF is translated, which suggested that PUMA-α is translated from an internal AUG. By experimenting with an inhibitor of CAP-dependent translation, I further demonstrated that PUMA-α translation is CAP-independent. Therefore, DNA damage is likely to activate certain translation re-initiation factors in order to stimulate PUMA-α protein accumulation, which is required to titrate out the anti-apoptotic BCL2 to induce intrinsic apoptosis.

5.2 Alternations of PUMA-α C-Terminus Reduces Cell Death Response to DNA Damage

In Chapter 3 of this thesis, I used the CRISPR/CAS9 double-cutting strategy to alter the C-terminal coding sequences of PUMA-α. I then examined 5-FU induced responses in three single cell clones, each with a differently modified C-terminus. Alterations of the C-terminal amino acids in the endogenous PUMA-α did not affect the induction of p53 and p21CIP1 expression by 5-FU, consistent with the fact that p53 acts upstream of PUMA-α and p21CIP1 is induced in parallel of PUMA-α in DNA damage response. Interestingly, however, in each of the three clones, with differently modified PUMA-α C-terminal amino acid, the 5-FU-induced

cleavage of pro-caspase-3 and PARP1 was reduced. Furthermore, 5-FU induced cell death was also reduced. When the three Δ*BBC3* clones were compared as a cohort to that consisting of the parental HCT116 cells and two control clones without editing, I found a statistically significant reduction in PARP1 cleavage and cell death percentage in the cohort with C-terminal alterations relative to the cohort with wild-type PUMA-α.

Previous studies using ectopic expressions of variously mutated PUMA-α cDNAs have found that the C-terminal amino acids (aa 164 to 193) contain a mitochondrial localization signal (MLS) that directs the insertion of PUMA-α into the outer membrane of mitochondria and this subcellular localization is important for PUMA-α to interact with BCL2, which is also localized to the mitochondrial outer membrane. In the three Δ*BBC3* clones I generated and characterized, the C-terminal modifications affecting the last 12 amino acids (aa 182-193) of PUMA-α, without altering the core membrane insertion alpha-helix (aa 167-176) in the MLS. Nevertheless, alterations of those C-terminal 12 amino acids in the endogenous PUMA-α in HCT116 cells appeared to be sufficient to reduce its pro-apoptotic activity.

The data presented in Chapter 3, however, did not elucidate the mechanism for how the three different alterations I introduced into the C-terminus of PUMA-α might have affected the pro-apoptotic function of this protein. An informative experiment that was not performed is to determine the subcellular localization of the C-terminal-modified PUMA-α proteins in the three Δ*BBC3* clones by immunofluorescence staining and subcellular fractionations (Andreu-Fernandez et al., 2016; Yee & Vousden, 2008)**.** Because I have verified the authenticity of two commercial anti-PUMA antibodies, they can be used to conduct the immunofluorescence and the fractionation experiments to determine whether the C-terminal-modified PUMA-α in the three Δ*BBC3* clones are in the mitochondria.

The data presented in Chapter 3 showed that the cell death response to 5-FU is significantly reduced but not abolished in the three Δ*BBC3* clones. With the current data, I cannot determine if this reduction is due to a partial or a complete loss of PUMA-α pro-apoptotic function. DNA damage-induced cell death in cancer cells can result from intrinsic apoptosis, extrinsic apoptosis, necroptosis, and mitotic catastrophe (Wang, 2019). In order to determine the contribution of PUMA-α to 5-FU-induced cell death, it is necessary to create a PUMA-α knockout HCT116 cells so that the cell death response can be compared between cells with wild-type PUMA-α, those without PUMA-α and those with the C-terminal-modified PUMA-α.

5.3 Expression of Venus and Neo Proteins from Exon-1a of *BBC3*

In Chapter 4 of the thesis, I applied the Endogenous Fluorescence Tagging (eFLUT) technology (Steward-Ornstein & Lahav, 2016) to insert an ORF of Venus_p2a_Neo (VpN) into Exon-1a and showed by live cell imaging and western blotting that Venus and Neo proteins were expressed in each of four Exon-1a edited clones characterized. These results suggested that an inserted ORF can be translated from Exon-1a. Due to failure to amplifying the 5'-junction between the PUMA-α uORF and the VpN-ORF from genomic DNA, I have not determined the sequence at the 5'-junction. As a result, I cannot conclude that it was the uORF AUG that initiated the translation of the VpN-ORF. In other words, the current results have not conclusively demonstrated that the uORF is translated. Rather than PCR/sequencing, next-generation sequencing technology may be applied to sequencing the whole exomes of the four E1a-edited clones so as to determine if the editing occurred in one or both alleles of the *BBC3* gene.

Given the observation that each of the four E1a-edited clones expressed the Venus, the Neo, and the PUMA-α proteins, it is tempting to conclude that translation from the uORF is not prohibitive of translation from the PUMA-α ORF. However, the current results fall short of supporting that conclusion because I have failed to demonstrate that the VpN-ORF was inserted into both alleles of *BBC3* (note that HCT116 cells are diploid, with two copies of the *BBC3* gene). It is possible that the VpN-insertion only occurred in one allele of the *BBC3* gene and that E1a-edited *BBC3* expressed Venus and Neo but not PUMA-α. In this scenario, translation of the VpN-ORF and the PUMA-α ORF would be from two different mRNAs; therefore, the effect of VpN-ORF on the translation of the PUMA-α ORF could not be determined. As a matter of fact, the current results also fall short of demonstrating that a bi-cistronic mRNA containing an upstream VpN-ORF and a downstream PUMA-α ORF was actually present in the E1a-edited clones. Detection of the bi-cistronic mRNA by RT-PCR also failed due to the high G/C-content of Exon-1a and Exon-2 sequences that make it difficult to design PCR primers and to carry out efficient PCR reactions. An alternative to RT-PCR/sequencing is to use the method of 5'-RACE (**R**apid **A**mplification of **c**DNA **E**nds) (Schramm et al., 2000) to generate cDNA clones of the expected bi-cistronic mRNA from the four Exon-1a-edited clones and then sequence those cDNA clones using universal primers that hybridize to sequences in the cloning vectors.

5.4 CAP-Independent Translation of PUMA-α

I have found that 4EGI-1, which disrupts the interaction of eIF-4E and eIF-4G to inhibit CAP-dependent translation initiation, did not inhibit 5-FU-induced expression of PUMA-α protein in HCT116 cells. This result strongly suggests that translation initiation of the PUMA-α ORF is CAP-independent. It would be of interest to determine how 4EGI-1 affects 5-FU-induced

expression of Neo protein in the four Exon-1a-edited clones, as the translation of the VpN-ORF should be CAP-dependent. This question can be readily addressed by the experimental protocol I have established. To further confirm that eIF-4E is not required for synthesis of PUMA-α protein, a complementary genetic approach to knockdown eIF-4E and eIF-4G by RNA-interference (RNAi) can be used. RNAi which was first discovered in the nematode C. *elegans*, has been widely used to knockdown gene expression either transiently or stably by using synthetic siRNA or by stable expression of shRNA (Haiyong, 2019; Fire et al., 1998). Previous studies have used the approach of eIF-4E and eIF-4G transient knockdown with siRNAs (Chen et al., 2015; Jaiswal et al., 2018) to determine their requirements for translation initiation of specific mRNAs. Experimental reagents and protocols established by those previous studies can be applied to determine their requirements for 5-FU to increase the levels of p53, p21CIP1, and PUMA-α in HCT116 cells.

The effect of 4EGI-1 on proteins was measured in my experiments by immunoblotting, which provides a rapid and sensitive assay for the detection of protein levels in whole cell lysates. Because the steady state level of a protein is determined by the rate of its synthesis and degradation, protein fold-change determined by immunoblotting cannot be simply ascribed to fold-change in translation. To definitively prove that PUMA-α translation is CAP-independent will require the direct measurement of protein synthesis by classical methods such as ^{35}S-Met pulse-labeling followed by immunoprecipitation and auto-radiography or by probing for PUMA-α RNA in the monosome and the polysome fractions of ribosomes. Alternatively, several advanced methods such as ribosome-profiling (Brar & Weissman, 2015) can be used to quantify ribosome-associated PUMA-α mRNA under conditions when CAP-dependent ribosome loading is inhibited to directly demonstrate that PUMA-α translation is CAP-independent.

5.5 Future Direction

Results from my thesis research have provided evidence to support the idea that translation of the PUMA-α ORF occurs from an internal AUG in a CAP-independent manner. If so, PUMA-α translation would require "re-initiation" factors for ribosome loading. My results add to our lab's previous finding that nuclear entry of the Abl tyrosine kinase is required for cisplatin to stimulate PUMA-α protein accumulation in mouse kidney epithelial cells, suggesting that nuclear Abl is required for the stimulation of PUMA-α translation (Sridevi et al., 2013). Identification of those factors that are required for the initiation of PUMA-α translation from its internal AUG is an important next step towards solving the mechanism by which nuclear Abl stimulates PUMA-α translation to activate intrinsic apoptosis in DNA damage response.

5.6 References

Andreu-Fernandez, V., Garcia-Murria, M., Bano-Polo, M., Martin, J., Monticelli, L., Orzaez, M., Mingarro, I. (2016). The C-terminal Domains of Apoptotic BH3-only Proteins Mediate Their Insertion into Distinct Biological Membranes. *The Journal of Biological Chemistry, 291(48),* 25207-25216. doi: 10.1074/jbc.M116.733634

Brar, G., Weissman, J. (2015). Ribosome profiling reveals the what, when, where and how of protein synthesis. *Nature, 16,* 651-664. doi: 10.1038/nrm4069

Chen, B., Zhang, B., Xia, L., Zhang, J., Chen, Y., Hu, Q., Zhu, C. (2015). Knockdown of eukaryotic translation initiation factor 4E suppresses cell growth and invasion, and induces apoptosis and cell cycle arrest in a human lung adenocarcinoma cell line. *Molecular Medicine Reports, 12(6),* 7971-7978. doi: 10.3892/mmr.2015.4468

Fire, A., Xu, S., Montgomery, M., Kostas, S., Driver, S., Mello, C. (1998). Potent and specific genetic interference by double-stranded RNA in Caenorhabditis elegans. *Nature, 391(6669),* 806-811. doi: 10.1038/35888

Haimov, O., Sehrawat, U., Tamarkin-Ben, A., Bahat, A., Uzonyi, A., Will, A., Hiraishi, H., Asano, K., Kikstein, R. (2018). Dynamic Interaction of Eukaryotic Initiation Factor 4G1 (eIF4G1) with eIF4E and eIF1 Underlies Scanning-Dependent and -Independent Translation. *Molecular and Cellular Biology, 38(18),* 1-15. doi: 10.1128/MCB.00139-18.

Haiyong, H. (2019). RNA Interference to Knock Down Gene Expression. *Methods in Molecular Biology, 1706,* 293-302. doi: 10.1007/978-1-4939-7471-9_16

Jaiswal, P., Koul, S., Shanmugam, P., Koul, H. (2018). Eukaryotic Translation Initiation Factor Gamma 1 (eIF4G1) is upregulated during Prostate cancer progression and modulates cell growth and metastasis. *Scientific Reports, 8(1),* 7459. doi: 10.1038/s41598-018-25798-7

Schramm, G., Bruchhaus, I., Roeder, T. (2000). A simple and reliable 5'-RACE approach. *Nucleic Acids Research, 28(22),* e96. doi: 10.1093/nar/28.22.e96

Sriram, A., Bohlen, J., Teleman, A. (2018). Translation acrobatics: how cancer cells exploit alternate modes of translation initiation. *EMBO reports, 10,* e45947. doi: 10.15252/embr.201845947

Wang, J. (2019). Cell Death Response to DNA Damage. *Yale Journal of Biology and Medicine, 92(4),* 771-779. PMID: 31866794

Yee, K., Vousden, K. (2008). Contribution of membrane localization to the apoptotic activity of PUMA. *Apoptosis, 13,* 87-95. doi: 10.1007/s10495-007-0140-2